J. Appl. Comput. Mech., 9(1) (2023) 239-258
DOI: 10.22055/jacm.2022.41265.3723

ISSN: 2383-4536
jacm.scu.ac.ir

Shahid Chamran University of Ahvaz

Journal of Applied and Computational Mechanics

Research Paper

Static Buckling of 2D FG Porous Plates Resting on Elastic Foundation based on Unified Shear Theories

Amr E. Assie[1,2], Salwa A. Mohamed[3], Rabab A. Shanab[4], Rasha M. Abo-bakr[5], Mohamed A. Eltaher[6,7]

[1] Mechanical Engineering Department, Faculty of Engineering, Jazan University, P. O. Box 45142, Jazan, Kingdom of Saudi Arabia
[2] Department of Mechanical Design and Production, Faculty of Engineering, Zagazig University, P.O. Box 44519, Zagazig, Egypt
[3] Department of Engineering Mathematics, Faculty of Engineering, Zagazig University, P.O. Box 44519, Zagazig, Egypt, Email: s_a_mohamed@hotmail.com
[4] Department of Engineering Mathematics, Faculty of Engineering, Zagazig University, P.O. Box 44519, Zagazig, Egypt, Email: rabab_shanab@zu.edu.eg
[5] Mathematical Department, Faculty of Science, Zagazig University, P.O. Box 44519, Zagazig, Egypt, Email: rasha_abobakr@hotmail.com
[6] Mechanical Dept., Faculty of Engineering, King Abdualziz University, Jeddah, Saudi Arabia, Email: mmeltaher@zu.edu.eg
[7] Mechanical Design and Production Dept., Faculty of Engineering, Zagazig University, Zagazig, Egypt, Email: mohaeltaher@gmail.com

Received July 04 2022; Revised August 07 2022; Accepted for publication August 24 2022.
Corresponding author: M.A. Eltaher (mmeltaher@zu.edu.eg)

Abstract. This article develops a mathematical model to study the static stability of bi-directional functionally graded porous unified plate (BDFGPUP) resting on elastic foundation. The power function distribution is proposed for the gradation of material constituent through thickness and axial directions. Three types of porosity are selected to portray the distribution of voids and cavities through the thickness of the plate. Unified theories of plate are exploited to present the kinematic fields and satisfy the zero-shear strain/stress at the top and bottom surfaces without shear correction factor. Hamilton's principle is employed to derive the governing equations of motions including the higher terms of force resultants. An efficient numerical method namely differential integral quadrature method (DIQM) is manipulated to discretize the structure spatial domain and transform the coupled variable coefficients partial differential equations to a system of algebraic equations. Problem validation and verification have been proven with previous works for bucking phenomenon. Parametric studies are exemplified to exhibit the significant impacts of kinematic shear relations, gradation indices, porosity type, and boundary conditions on the static stability and buckling loads of BDFGP plate. The proposed model is economical in different applications in nuclear, mechanical, aerospace, naval, dental and medical fields.

Keywords: Buckling; Bi-directional functional graded; Unified plate theories; Porous structurers; Differential integral quadrature method.

1. Introduction

Recently, advanced aerospace vehicles, nuclear reactors, naval, electronics and biomedical structures are operated under tremendous loading and high thermal and moisture environmental conditions. Therefore, functionally graded materials (FGMs) with enhanced properties such as lightweight, high stiffness, high-temperature resistance are exploited in these applications to overcome the disadvantages of classical composites (i.e., high interfacial stress concentrations, the crack formation, delamination, moisture sensitivity) [1, 2]. FGM which were invented during the space-plane project in Japan 1984 [3], can be used as thermal barrier capable of withstanding a surface temperature of 2000 K and a temperature gradient of 1000 K across a cross-section of size < 10 mm [4].

In some applications such as aerospace craft, nuclear and shuttles, distributions of the stress or thermal field in the structural elements of such advanced machines can be in two or three directions and thus, the conventional 1D FGMs are not sufficient. As a consequence, there is a need for multi-directional FGMs [5]. Wu and Huang [6] developed a semi-analytical finite element method to evaluate the stress and deformation of 2D FG truncated conical shells. Abo-Bakr et al. [7-9] evaluated the optimum weight of FG microbeam under the buckling and free vibrations constraints using multiobjective shape optimization. Abo-Bakr et al. [10] developed multi-objective optimization for lightweight design of 2D FG beams for maximum frequency and buckling load by using semi-analytical method. Pham et al. [11] exploited the isogeometric analysis (IGA) in free vibration analysis of bidirectional functionally graded (BDFG) rectangular plates in the fluid medium using power-law distributions and Mori-Tanaka model. Attia and Shanab [12, 13] studied the bending, buckling, and vibration characteristics of 2D FGM nanobeams with couple

Published online: September 05 2022

stress and surface energy using Navier analytical solution. Chen et al. [14] investigated the nonlinear forced response 2D FGM plate with global and localized geometrical imperfections in the frame of Kirchhoff hypothesis and von Kármán's nonlinear strain. Hendi et al. [15] studied nonlinear thermal vibration of pre/post-buckled two-dimensional FGM tapered microbeams based higher deformation theory. Ohab-Yazdi et al. [16] studied the vibration of 2D-FG rotary nonlocal nanobeam with even porosity distribution by generalized differential quadrature method (GDQM). Abo-Bakr et al. [9] obtained the optimal weight of FG beam structures under the variable axial loads based on the critical buckling constraint. Banh et al. [17] introduced a multigrid preconditioned conjugate gradient-oriented topology optimization methodology using multiple 2D FG models. Arasan et al. [18] presented a general solution to 2D elastic problems involving FGMs in radial co-ordinates with arbitrary geometry and boundary/loading conditions. Fu et al. [19] used the conjugate gradient method and fast Fourier transform to evaluate elastic shakedown limit of 2D thermo-elastic rolling/sliding contact for FG coating/substrate structure. Brischetto and Torre [20] investigated the 3D stress analysis of multilayered FG plates and shells under moisture conditions using exact layer-wise approach. Barati et al. [21] studied the vibration 2D FG nonlocal nanobeams under magnetic field using generalized differential quadrature method.

The choice of displacement fields and transverse shear functions used in analyzing of beam and plate theories is critical to the accuracy of the obtained results. Even though, the fundamental of classical plate theory developed by Kirchhoff-Love is missing the influence of shear strain and hence the shear stress, [22]. Reddy [23] adopted the Mindlin's plate theory for isotropic plates to consider laminated anisotropic plates and include shear deformation and rotary inertia effects. In 1991 Touratier [24] exploited a classic plate theory with cosine shear stress distribution to study the mechanical behaviors of laminates and sandwich composite plates. Assie and Mahmoud [25] exploited a first order shear deformation and finite element method to investigate the dynamic response of thick hygrothermal viscoelastic composite laminates. Mantari et al. [26] investigated the bending response of FG plates by using a new higher order shear deformation theory as a combination of exponential and trigonometric functions of the thickness coordinate. Neves et al [27] considered the Zig-Zag and warping effects in studying the bending behavior of FG sandwich plates using a hyperbolic theory of plate. Sedighi et al. [28, 29] developed an analytical solution of the nonlinear vibration of buckled beam with generalized deadzone discontinuity. Mantari and Soares [30] included stretching effect in analyzing the static bending of FG plate using a new trigonometric shear deformation function. Assie et al. [31] presented an integrated model for optimum weight design of symmetrically laminated composite plates subjected to dynamic excitation using first order shear deformation theory. Yu et al. [32] studied the buckling and free vibration of laminated composites plates with cutouts by using a new simple first order shear deformation with 4 variables. Nguyen et al. [33] investigated analytically the bending and vibration of FG plates based on a refined simple first-order shear deformation theory. Vu et al. [34] developed a refined quasi-3D logarithmic shear deformation theory to study the mechanical response of isotropic and FG plates laid on elastic foundation. Raissi [35] used layerwise plate theory to investigate stress s in adhesive layers of a five-layer circular sandwich plate subjected to temperature gradient. Based on quasi-3D higher shear deformation theory with five unknowns (HSDT), Khiloun et al. [36] developed an analytical solution to study a bending and vibration of thick advanced composite plates using a four-variable quasi 3D HSDT. Fallahi et al. [37] studied free vibration, and static analyses of variable angle tow panels in the framework of the Carrera unified formulation. Fallahi [38] optimized the buckling and free vibration response of variable angle tow composites through layerwise theory.

Arshid et al. [39] examined a vibration of FG porous modified couple stress microplates under hygrothermal effect. Pham et al. [40] exploited finite element method and a quasi-3D nonlocal theory to analysis the vibration of FGM nanoplates rested on elastic foundations in the thermal environment. Pavlovic et al. [41] studied the buckling response telescopic boom using finite element method by ANSYS. Daikh et al. [42,43] studied static and dynamic stability responses of sigmoidal FG and multilayer FG carbon nanotubes reinforced composite nanoplates using nonlocal strain gradient theory. Li et al. [44] analyzed the vibration response of FGM plates rested on Winkler/Pasternak/Kerr foundations using a new logarithmic shape function quasi-3D HSDT. Van [45] exploited hybrid quasi-3D plate theory to study the bending and vibration of 2D FGM sandwich plate laid on Pasternak's elastic foundations. The unified plate theories are exploited in many studied, such as, Daik et al. [43] examined the static buckling and bending stability of axially temperature-dependent FG carbon nanotube reinforced composite plates. Sadgui and Tati [46] used a trigonometric shear deformation theory in analyzing of buckling and free vibration of FG plates. Li et al. [47] presented a comparative analysis on higher-order shear deformation theories based on the existing shear deformation functions. Tran et al. [48] studied the vibration of FG plates resting on the elastic foundation in the thermal environment by using first order shear deformation theory. Sofiyev and Dikmen [49] evaluated the critical buckling loads of FG shells under mixed boundary conditions subjected to uniform lateral pressure. Civalek and Avcar [50] analyzed buckling and vibration response of CNT reinforced laminated non-rectangular plates by discrete singular convolution method.

During fabrication of FGM, voids may be generated during sintering because of difference in solidification temperatures of materials. Voids and porosities have adverse effects on required properties of structures. In other case, representative porous materials extensively used in lightweight structures, aerospace and automotive industries, due to their outstanding multi-functionality obtained by low density, efficient capacity of energy dissipation, reduced thermal and electrical conductivity, [51]. Different types of porous structures have been widely studied, [52]. Sobhy and Zenkour [53] used modified exponential porosity model to investigate the porosity and inhomogeneity effects on buckling and vibration of double FGM nanoplates. On the basis of cosine symmetric and antisymmetric porosity models, Coskun et al. [54] studied the mechanical response of FG porous modified couple stress microplates using a general third order plate theory. Kim et al. [55] investigated the bending, buckling and vibration of FG porous microplates based on classical and first-order shear deformation plate theories. Hamed et al. [51] analyzed the buckling stability of FG porous beam under variable axial load. Babaei et al. [56] studied the static and vibration responses of FG porous annular elliptical sector plate based on 3D finite element method, where the porosity defined by nonlinear symmetric, nonsymmetric and uniform functions. Esmaeilzadeh et al. [57] investigated the nonlinear dynamic of 2D FG porous nanoplate in the frame of a nonlocal strain gradient model. Cho [58] studied the interaction of oblique incident waves with a floating porous plate using the matched eigenfunction expansion method and Darcy's law for the porous boundary condition. Hieu et al. [59] investigated the nonlinear bending, buckling and vibration of FG nanobeams resting on an elastic foundation in the frame of nonlocal strain gradient. Katiyar and Gupta [60] investigated the vibration of FG porous plate rested on elastic foundation and subjected to thermal influence by using refined non-polynomial trigonometric higher-order shear deformation theory. Abdollahi et al. [52] exploited power law with uniform porosity distribution to study aeroelastic behavior of honeycomb sandwich plates with FG porous faces. Akbaş et al. [61,62] studied the dynamic response of viscoelastic FG porous thick beams under pulse load. Sah and Ghosh [63] studied free vibration and buckling of multi-directional FG sandwich plates with porosity using even and uneven functional distributions.

Based on the previous works and literature survey, the buckling static stability of bidirectional FG porous plate surrounded by elastic foundation and modelled by unified higher order shear plate theories has not been addressed. Therefore, this article aims to present this topic in comprehensive analysis. The rest of the article is organized as following: - the problem formulation including the kinematic displacement filed, constitutive relations, porosity models, equilibrium equations, and boundary conditions are developed in section 2. Section 3 presents a solution methodology, a discretization of spatial coordinates, formulations of geometrical and stiffness matrices. Model validations numerical results, and parametric studies are discussed through section 4. Conclusions and main features are summarized in section 5.

2. Problem Formulation

2.1 A general kinematic field

The displacement field based on four variables high-order shear deformation theory with no shear correction factors can be expressed as:

$$u(x,y,z)=u_o(x,y)-z\frac{\partial w_b}{\partial x}-F(z)\frac{\partial w_s}{\partial x} \tag{1.a}$$

$$v(x,y,z)=v_o(x,y)-z\frac{\partial w_b}{\partial y}-F(z)\frac{\partial w_s}{\partial y} \tag{1.b}$$

$$w(x,y,z)=w_b(x,y)+w_s(x,y) \tag{1.c}$$

where:

- u_o , v_o , w_b and w_s are the displacements defined at the midplane.
- w_b and w_s stand for bending and shear parts, respectively.
- $F(z)$ is a shape function that estimates the distribution of transverse shear.

The proposed unified theories are based on single equivalent layer theory; therefore, several forms are adopted to describe adequately the change of the transverse shear strain across the thickness direction as shown in Table 1.

The normal and shear strains associated with the displacement field portrayed by Eq. (1) are:

$$\begin{gathered}\varepsilon_x=\varepsilon_x^0-z\frac{\partial^2 w_b}{\partial x^2}-F(z)\frac{\partial^2 w_s}{\partial x^2},\qquad \varepsilon_y=\varepsilon_y^0-z\frac{\partial^2 w_b}{\partial y^2}-F(z)\frac{\partial^2 w_s}{\partial y^2},\\ \gamma_{xy}=\gamma_{xy}^0-z\left(2\frac{\partial^2 w_b}{\partial x\partial y}\right)-F(z)\left(2\frac{\partial^2 w_s}{\partial x\partial y}\right),\qquad \gamma_{yz}=G(z)\frac{\partial w_s}{\partial y},\qquad \gamma_{xz}=G(z)\frac{\partial w_s}{\partial x}\end{gathered} \tag{2}$$

where

$$\varepsilon_x^o=\frac{\partial u_o}{\partial x},\ \varepsilon_y^o=\frac{\partial v_o}{\partial y},\quad \text{and}\quad \gamma_{xy}^o=\frac{\partial u_o}{\partial y}+\frac{\partial v_o}{\partial x} \tag{3.a}$$

$$F(z)=z-f(z)\quad \text{and}\quad G(z)=1-F'(z)=f'(z) \tag{3.b}$$

2.2 Constitutive equations

The stress-strain constitutive relations (plane stress) for 2D shear deformation plate theory $\varepsilon_z=0$ under isothermal conditions can be defined by:

$$\begin{bmatrix}\sigma_x\\ \sigma_y\\ \tau_{xy}\\ \tau_{yz}\\ \tau_{xz}\end{bmatrix}=\begin{bmatrix}Q_{11}&Q_{12}&0&0&0\\ Q_{12}&Q_{22}&0&0&0\\ 0&0&Q_{66}&0&0\\ 0&0&0&Q_{44}&0\\ 0&0&0&0&Q_{55}\end{bmatrix}\begin{bmatrix}\varepsilon_x\\ \varepsilon_y\\ \gamma_{xy}\\ \gamma_{yz}\\ \gamma_{xz}\end{bmatrix} \tag{4.a}$$

Table 1. Forms of the transversal shear strain shape functions $F(z)$

	Reference	$F(z)$
1	**Touratier [24]**	$z-\left(\frac{h}{\pi}\right)\sin\left(\frac{\pi z}{h}\right)$
2	**Karama et al. [64]**	$z\left(1-e^{-2\left(\frac{z}{h}\right)^2}\right)$
3	**Reddy [23]**	$\frac{4z^3}{3h^2}$
4	**Thai and Kim [65]**	$z\left(-\frac{1}{4}+\frac{5}{3}\frac{z^2}{h^2}\right)$
5	**Taibi et al. [66]**	$\frac{\frac{h}{\pi}\sinh\left(\frac{\pi z}{h}\right)-z}{\cosh\left(\frac{\pi}{2}\right)-1}$

For isotropic materials, the plane stress stiffnesses are:

$$Q_{11} = Q_{22} = \frac{E}{1-\nu^2}, \quad Q_{12} = \frac{\nu E}{1-\nu^2} \tag{4.b}$$

$$Q_{44} = Q_{55} = Q_{66} = \frac{E}{2(1+\nu)} \tag{4.c}$$

where E is the Young modulus and ν is the Poisson's ratio. By assuming that, the FG material properties are graded in both axial directions (x -axis) and transverse directions (z -axis) according to power law and including porosity and voids as:

$$P(x,z,\phi) = [P_m + P_{cm}\left(\frac{1}{2}+\frac{z}{h}\right)^{n_z}\left(\frac{x}{a}\right)^{n_x}[1-\Phi(z)] \tag{5.a}$$

$$P_{cm} = P_c - P_m \tag{5.b}$$

in which P denotes a generic material property like E that variates in z- and x-directions according to power laws with indices, n_z and n_x. The subscript c and m represent the ceramics and metals constitutions, respectively. Poisson's ratio, ν is assumed to be constant. The porosity distribution function $\Phi(z)$ has been proposed to have the following three forms:

Type 1 (center enhanced): $$\Phi(z) = \phi\cos\left(\frac{\pi}{h}z\right) \tag{6.a}$$

Type 2 (top enhanced): $$\Phi(z) = \phi\cos\left(\frac{\pi}{2}\left(\frac{z}{h}+\frac{1}{2}\right)\right) \tag{6.b}$$

Type 3 (bottom enhanced): $$\Phi(z) = \phi\cos\left(\frac{\pi}{2}\left(\frac{z}{h}-\frac{1}{2}\right)\right) \tag{6.c}$$

in which ϕ is the porosity coefficient.

2.3 A general kinematic field

The governing equilibrium equations and associated boundary conditions of the developed model are derived on the basis of Hamilton's Principles, which states:

$$\int_0^T \delta\left(U + V + U_{ef} - K\right)dt = 0 \tag{7}$$

The virtual potential work of applied in-plane loads can be expressed in the form δV :

$$\delta V = \int_A \left(N_x^o \frac{\partial\bar{w}}{\partial x}\frac{\partial\delta\bar{w}}{\partial x} + N_{xy}^o\left(\frac{\partial\bar{w}}{\partial x}\frac{\partial\delta\bar{w}}{\partial y} + \frac{\partial\bar{w}}{\partial y}\frac{\partial\delta\bar{w}}{\partial x}\right) + N_y^o \frac{\partial\bar{w}}{\partial y}\frac{\partial\delta\bar{w}}{\partial y}\right)dA \tag{8.a}$$

The variation, δV using Hamilton's Principles results in the following:

$$w = \bar{w} = w_b + w_s \tag{8.b}$$

The variation of potential energy of the elastic foundation (Winkler -Pasternak type as shown in Fig. 1) can be expressed as:

$$\delta U_{ef} = \int_A [K_w(w_b + w_s) - K_p\nabla^2(w_b + w_s)]\delta(w_b + w_s)dA \tag{8.c}$$

where $\nabla^2(w_b + w_s) = \partial^2(w_b + w_s)/\partial x^2 + \partial^2(w_b + w_s)/\partial y^2$.

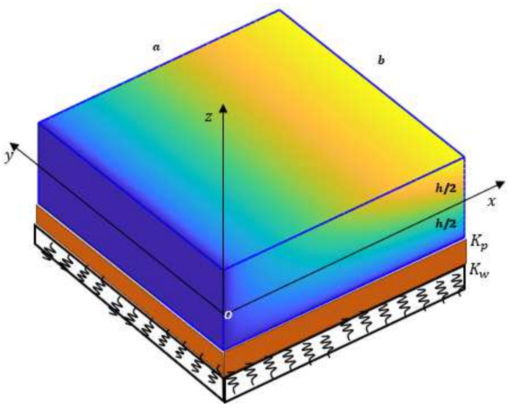

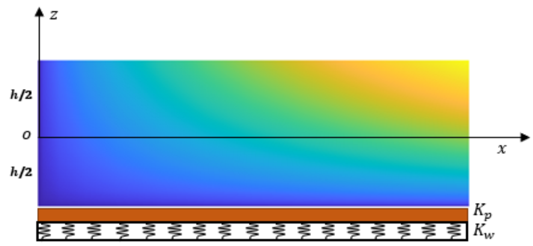

Fig. 1. Geometrical dimension of 2D FG plate rested on elastic Winkler-Pasternak foundation at gradation indices $n_x = n_z = 0.5$

Because of the static analysis will be considered only through this analysis, the virtual Kinetic Energy can be presented as:

$$\delta K = 0 \tag{9}$$

The virtual strain energy δU:

$$\delta U = \int_V \left(\sigma_x \delta\varepsilon_x + \sigma_y \delta\varepsilon_y + \tau_{xy}\delta\gamma_{xy} + \tau_{xz}\delta\gamma_{xz} + \tau_{yz}\delta\gamma_{yz}\right) dV \tag{10.a}$$

The virtual strain energy, δU in terms of stress resultants is derived as:

$$\delta U = \int_A \left[N_x \delta\varepsilon_x^0 + N_y \delta\varepsilon_y^0 + N_{xy}\delta\gamma_{xy}^0 - M_x^b \frac{\partial^2 \delta w_b}{\partial x^2} - M_y^b \frac{\partial^2 \delta w_b}{\partial y^2} - M_{xy}^b\left(2\frac{\partial^2 \delta w_b}{\partial x \partial y}\right) - M_x^s \frac{\partial^2 \delta w_s}{\partial x^2} - M_y^s \frac{\partial^2 \delta w_s}{\partial y^2} - M_{xy}^s\left(2\frac{\partial^2 \delta w_s}{\partial x \partial y}\right) + S_{yz}^s \frac{\partial \delta w_s}{\partial y} + S_{xz}^s \frac{\partial \delta w_s}{\partial x} \right] dA \tag{10.b}$$

where, the stress resultants can be expressed in terms of generalized displacements (u_0, v_0, w_b, w_s) in a matrix form:

$$\begin{bmatrix} N_x \\ N_y \\ N_{xy} \\ M_x^b \\ M_y^b \\ M_{xy}^b \\ M_x^s \\ M_y^s \\ M_{xy}^s \end{bmatrix} = \begin{bmatrix} A_{11} & A_{12} & 0 & B_{11} & B_{12} & 0 & B_{11}^s & D_{12}^s & 0 \\ A_{12} & A_{22} & 0 & B_{12} & B_{22} & 0 & B_{12}^s & B_{22}^s & 0 \\ 0 & 0 & A_{66} & 0 & 0 & B_{66} & 0 & 0 & B_{66}^s \\ B_{11} & B_{12} & 0 & D_{11} & D_{12} & 0 & D_{11}^s & D_{12}^s & 0 \\ B_{12} & B_{22} & 0 & D_{12} & D_{22} & 0 & D_{12}^s & D_{22}^s & 0 \\ 0 & 0 & B_{66} & 0 & 0 & D_{66} & 0 & 0 & D_{66}^s \\ B_{11}^s & B_{12}^s & 0 & D_{11}^s & D_{12}^s & 0 & H_{11}^s & H_{12}^s & 0 \\ B_{12}^s & B_{22}^s & 0 & D_{12}^s & D_{22}^s & 0 & H_{12}^s & H_{22}^s & 0 \\ 0 & 0 & B_{66}^s & 0 & 0 & D_{66}^s & 0 & 0 & H_{66}^s \end{bmatrix} \begin{bmatrix} \partial u_0 / \partial x \\ \partial v_0 / \partial y \\ (\partial u_0 / \partial y) + (\partial v_0 / \partial x) \\ -\partial^2 w_b / \partial^2 x \\ -\partial^2 w_b / \partial^2 y \\ -2\partial^2 w_b / \partial x \partial y \\ -\partial^2 w_s / \partial^2 x \\ -\partial^2 w_s / \partial^2 y \\ -2\partial^2 w_s / \partial x \partial y \end{bmatrix} \tag{11.a}$$

$$\begin{bmatrix} S_{yz}^s \\ S_{xz}^s \end{bmatrix} = \begin{bmatrix} A_{44}^s & 0 \\ 0 & A_{55}^s \end{bmatrix} \begin{bmatrix} \partial w_s / \partial y \\ \partial w_s / \partial x \end{bmatrix} \tag{11.b}$$

Rigidities terms are obtained as functions of x by:

$$\left[A_{ij}(x), B_{ij}(x), D_{ij}(x), B_{ij}^s(x), D_{ij}^s(x),\ H_{ij}^s(x)\right] = \int_{-h/2}^{h/2} Q_{ij}(x,z)\left[1, z, z^2, F(z), zF(z), (F(z))^2\right] dz \quad ij = 11, 12, 22, 66 \tag{12.a}$$

$$A_{ij}^s(x) = \int_{-h/2}^{h/2} Q_{ij}(x,z)(G(z))^2 dz\ ,\ ij = 44, 55 \tag{12.b}$$

where $Q_{ij}(x,z)$ and $E(x,z)$ are defined by Eqs. (4) and (5.a), respectively. Substituting Eqs. (8), (9) and (10) for δV, δK and δU, respectively, into Eq. (7) and performing integration by parts, the equations of FGM porous plate in terms of stress resultants are obtained as:

$$\delta u_o: \quad \frac{\partial N_x}{\partial x} + \frac{\partial N_{xy}}{\partial y} = 0 \tag{13.a}$$

$$\delta v_o: \quad \frac{\partial N_{xy}}{\partial x} + \frac{\partial N_y}{\partial y} = 0 \tag{13.b}$$

$$\delta w_b: \quad \frac{\partial^2 M_x^b}{\partial x^2} + 2\frac{\partial^2 M_{xy}^b}{\partial x \partial y} + \frac{\partial^2 M_y^b}{\partial y^2} + \bar{N}^o + K_P \nabla^2 (w_b + w_s) - K_w (w_b + w_s) = 0 \tag{13.c}$$

$$\delta w_s: \quad \frac{\partial^2 M_x^s}{\partial x^2} + 2\frac{\partial^2 M_{xy}^s}{\partial x \partial y} + \frac{\partial^2 M_y^s}{\partial y^2} + \frac{\partial S_{yz}^s}{\partial y} + \frac{\partial S_{xz}^s}{\partial x} + \bar{N}^o + K_P \nabla^2 (w_b + w_s) - K_w (w_b + w_s) = 0 \tag{13.d}$$

associated with the following boundary conditions:

$$\delta u_0: \quad N_x \bar{n}_x + N_{xy}\bar{n}_y = 0 \tag{14.a}$$

$$\delta v_o: \quad N_{xy}\bar{n}_x + N_y \bar{n}_y = 0 \tag{14.b}$$

$$\delta w_b: \quad \left(M_{x,x}^b + M_{xy,y}^b\right)\bar{n}_x + \left(M_{xy,x}^b + M_{y,y}^b\right)\bar{n}_y + P(\bar{w}) = 0 \tag{14.c}$$

$$\frac{\partial \delta w_b}{\partial x}: \quad M_x^b \bar{n}_x + M_{xy}^b \bar{n}_y = 0 \tag{14.d}$$

$$\frac{\partial \delta w_b}{\partial y}: \quad M_{xy}^b \bar{n}_x + M_y^b \bar{n}_y = 0 \tag{14.e}$$

$$\delta w_s: \quad \left(M^s_{x,x} + M^s_{xy,y} + S^s_{xz}\right)\bar{n}_x + \left(M^s_{xy,x} + M^s_{y,y} + S^s_{yz}\right)\bar{n}_y + P(\bar{w}) = 0 \tag{14.f}$$

$$\frac{\partial \delta w_s}{\partial x}: \qquad M^s_x \bar{n}_x + M^s_{xy}\bar{n}_y = 0 \tag{14.g}$$

$$\frac{\partial \delta w_s}{\partial y}: \qquad M^s_{xy} \bar{n}_x + M^s_{y}\bar{n}_y = 0 \tag{14.h}$$

$$P(\bar{w}) = \left(N^o_x \frac{\partial(\bar{w})}{\partial x} + N^o_{xy}\frac{\partial(\bar{w})}{\partial y}\right)\bar{n}_x + \left(N^o_{xy}\frac{\partial(\bar{w})}{\partial x} + N^o_y \frac{\partial(\bar{w})}{\partial y}\right)\bar{n}_y \tag{14.i}$$

By substituting Eqs. (2), (3) and (11) into Eq. (13), the governing equilibrium equations can be acquired in terms of displacements, as following:

$$\begin{aligned}
\delta u_0 : & \mathbf{A}_{11}(\mathbf{x})\frac{\partial^2 \mathbf{u}_0}{\partial \mathbf{x}^2} + \left(\mathbf{A}_{12}(\mathbf{x}) + \mathbf{A}_{66}(\mathbf{x})\right)\frac{\partial^2 \mathbf{v}_0}{\partial \mathbf{x}\partial \mathbf{y}} + \mathbf{A}_{66}(\mathbf{x})\frac{\partial^2 \mathbf{u}_0}{\partial \mathbf{y}^2} + \mathbf{A}'_{11}(\mathbf{x})\frac{\partial \mathbf{u}_0}{\partial \mathbf{x}} + \mathbf{A}'_{12}(\mathbf{x})\frac{\partial \mathbf{v}_0}{\partial \mathbf{y}} \\
& - \left(\mathbf{B}_{12}(\mathbf{x}) + 2\,\mathbf{B}_{66}(\mathbf{x})\right)\frac{\partial^3 \mathbf{w_b}}{\partial \mathbf{x}\partial \mathbf{y}^2} - \left(\mathbf{B}^s_{12}(\mathbf{x}) + 2\,\mathbf{B}^s{}_{66}(\mathbf{x})\right)\frac{\partial^3 \mathbf{w_s}}{\partial \mathbf{x}\partial \mathbf{y}^2} - \mathbf{B}_{11}(\mathbf{x})\frac{\partial^3 \mathbf{w_b}}{\partial \mathbf{x}^3} - \mathbf{B}^s_{11}(\mathbf{x})\frac{\partial^3 \mathbf{w_s}}{\partial \mathbf{x}^3} \\
& - \mathbf{B}'_{11}(\mathbf{x})\frac{\partial^2 \mathbf{w_b}}{\partial \mathbf{x}^2} - \mathbf{B}'_{12}(\mathbf{x})\frac{\partial^2 \mathbf{w_b}}{\partial \mathbf{y}^2} - \mathbf{B}^{s'}_{11}(\mathbf{x})\frac{\partial^2 \mathbf{w_s}}{\partial \mathbf{x}^2} - \mathbf{B}^{s'}_{12}(\mathbf{x})\frac{\partial^2 \mathbf{w_s}}{\partial \mathbf{y}^2} = 0
\end{aligned} \tag{15}$$

$$\begin{aligned}
\delta v_0 : & \mathbf{A}_{22}(\mathbf{x})\frac{\partial^2 \mathbf{v}_0}{\partial \mathbf{y}^2} + \left(\mathbf{A}_{12}(\mathbf{x}) + \mathbf{A}_{66}(\mathbf{x})\right)\frac{\partial^2 \mathbf{u}_0}{\partial \mathbf{x}\partial \mathbf{y}} + \mathbf{A}_{66}(\mathbf{x})\frac{\partial^2 \mathbf{v}_0}{\partial \mathbf{x}^2} + \mathbf{A}'_{66}(\mathbf{x})\left(\frac{\partial \mathbf{u}_0}{\partial \mathbf{y}} + \frac{\partial \mathbf{v}_0}{\partial \mathbf{x}}\right) \\
& - \left(\mathbf{B}_{12}(\mathbf{x}) + 2\mathbf{B}_{66}(\mathbf{x})\right)\frac{\partial^3 \mathbf{w_b}}{\partial \mathbf{x}^2\partial \mathbf{y}} - \left(\mathbf{B}^s_{12}(\mathbf{x}) + 2\mathbf{B}^s_{66}(\mathbf{x})\right)\frac{\partial^3 \mathbf{w_s}}{\partial \mathbf{x}^2\partial \mathbf{y}} - \mathbf{B}_{22}(\mathbf{x})\frac{\partial^3 \mathbf{w_b}}{\partial \mathbf{y}^3} \\
& - \mathbf{B}^s_{22}(\mathbf{x})\frac{\partial^3 \mathbf{w_s}}{\partial \mathbf{y}^3} - 2\mathbf{B}'_{66}(\mathbf{x})\frac{\partial^2 \mathbf{w_b}}{\partial \mathbf{x}\partial \mathbf{y}} - 2\mathbf{B}^{s'}_{66}(\mathbf{x})\frac{\partial^2 \mathbf{w_s}}{\partial \mathbf{x}\partial \mathbf{y}} = 0
\end{aligned} \tag{16}$$

$$\begin{aligned}
\delta w_b : & \mathbf{B}_{11}(\mathbf{x})\frac{\partial^3 \mathbf{u}_0}{\partial \mathbf{x}^3} + \mathbf{B}_{22}(\mathbf{x})\frac{\partial^3 \mathbf{v}_0}{\partial \mathbf{y}^3} + \left(\mathbf{B}_{12}(\mathbf{x}) + 2\mathbf{B}_{66}(\mathbf{x})\right)\left(\frac{\partial^3 \mathbf{u}_0}{\partial \mathbf{x}\partial \mathbf{y}^2} + \frac{\partial^3 \mathbf{v}_0}{\partial \mathbf{x}^2\partial \mathbf{y}}\right) + 2\left(\mathbf{B}'_{12}(\mathbf{x}) + \mathbf{B}'_{66}(\mathbf{x})\right)\frac{\partial^2 \mathbf{v}_0}{\partial \mathbf{x}\partial \mathbf{y}} \\
& + 2\mathbf{B}'_{66}(\mathbf{x})\frac{\partial^2 \mathbf{u}_0}{\partial \mathbf{y}^2} + 2\mathbf{B}'_{11}(\mathbf{x})\frac{\partial^2 \mathbf{u}_0}{\partial \mathbf{x}^2} + \mathbf{B}''_{11}(\mathbf{x})\frac{\partial \mathbf{u}_0}{\partial \mathbf{x}} + \mathbf{B}''_{12}(\mathbf{x})\frac{\partial \mathbf{v}_0}{\partial \mathbf{y}} - \mathbf{D}_{11}(\mathbf{x})\frac{\partial^4 \mathbf{w_b}}{\partial \mathbf{x}^4} - \mathbf{D}_{22}(\mathbf{x})\frac{\partial^4 \mathbf{w_b}}{\partial \mathbf{y}^4} - \mathbf{D}^s_{22}(\mathbf{x})\frac{\partial^4 \mathbf{w_s}}{\partial \mathbf{y}^4} \\
& - 2\left(\mathbf{D}_{12}(\mathbf{x}) + 2\mathbf{D}_{66}(\mathbf{x})\right)\frac{\partial^4 \mathbf{w_b}}{\partial \mathbf{x}^2\partial \mathbf{y}^2} - 2\left(\mathbf{D}^s_{12}(\mathbf{x}) + 2\mathbf{D}^s_{66}(\mathbf{x})\right)\frac{\partial^4 \mathbf{w_s}}{\partial \mathbf{x}^2\partial \mathbf{y}^2} - \mathbf{D}^s_{11}(\mathbf{x})\frac{\partial^4 \mathbf{w_s}}{\partial \mathbf{x}^4} - 2\left(\mathbf{D}'_{12}(\mathbf{x}) + 2\mathbf{D}'_{66}(\mathbf{x})\right)\frac{\partial^3 \mathbf{w_b}}{\partial \mathbf{x}\partial \mathbf{y}^2} \\
& - 2\left(\mathbf{D}^{s'}_{12}(\mathbf{x}) + 2\mathbf{D}^{s'}_{66}(\mathbf{x})\right)\frac{\partial^3 \mathbf{w_s}}{\partial \mathbf{x}\partial \mathbf{y}^2} - 2\mathbf{D}'_{11}(\mathbf{x})\frac{\partial^3 \mathbf{w_b}}{\partial \mathbf{x}^3} - 2\mathbf{D}^{s'}_{11}(\mathbf{x})\frac{\partial^3 \mathbf{w_s}}{\partial \mathbf{x}^3} - \mathbf{D}''_{11}(\mathbf{x})\frac{\partial^2 \mathbf{w_b}}{\partial \mathbf{x}^2} - \mathbf{D}^{s''}_{11}(\mathbf{x})\frac{\partial^2 \mathbf{w_s}}{\partial \mathbf{x}^2} - \mathbf{D}''_{12}(\mathbf{x})\frac{\partial^2 \mathbf{w_b}}{\partial \mathbf{y}^2} \\
& - \mathbf{D}^{s''}_{12}(\mathbf{x})\frac{\partial^2 \mathbf{w_s}}{\partial \mathbf{y}^2} + \bar{N}^0 + K_p\nabla^2(\mathbf{w_b} + \mathbf{w_s}) - K_w(\mathbf{w_b} + \mathbf{w_s}) = 0
\end{aligned} \tag{17}$$

$$\begin{aligned}
\delta w_s : & \mathbf{B}^s_{11}(\mathbf{x})\frac{\partial^3 \mathbf{u}_0}{\partial \mathbf{x}^3} + \mathbf{B}^s_{22}(\mathbf{x})\frac{\partial^3 \mathbf{v}_0}{\partial \mathbf{y}^3} + \left(\mathbf{B}^s_{12}(\mathbf{x}) + 2\mathbf{B}^s_{66}(\mathbf{x})\right)\left(\frac{\partial^3 \mathbf{u}_0}{\partial \mathbf{x}\partial \mathbf{y}^2} + \frac{\partial^3 \mathbf{v}_0}{\partial \mathbf{x}^2\partial \mathbf{y}}\right) + 2\left(\mathbf{B}^{s'}_{12}(\mathbf{x}) + \mathbf{B}^{s'}_{66}(\mathbf{x})\right)\frac{\partial^2 \mathbf{v}_0}{\partial \mathbf{x}\partial \mathbf{y}} \\
& + 2\mathbf{B}^{s'}_{66}(\mathbf{x})\frac{\partial^2 \mathbf{u}_0}{\partial \mathbf{y}^2} + 2\mathbf{B}^{s'}_{11}(\mathbf{x})\frac{\partial^2 \mathbf{u}_0}{\partial \mathbf{x}^2} + \mathbf{B}^{s''}_{11}(\mathbf{x})\frac{\partial \mathbf{u}_0}{\partial \mathbf{x}} + \mathbf{B}^{s''}_{12}(\mathbf{x})\frac{\partial \mathbf{v}_0}{\partial \mathbf{y}} - \mathbf{D}^s_{11}(\mathbf{x})\frac{\partial^4 \mathbf{w_b}}{\partial \mathbf{x}^4} - \mathbf{D}^s_{22}(\mathbf{x})\frac{\partial^4 \mathbf{w_b}}{\partial \mathbf{y}^4} \\
& - 2\left(\mathbf{D}^s_{12}(\mathbf{x}) + 2\mathbf{D}^s_{66}(\mathbf{x})\right)\frac{\partial^4 \mathbf{w_b}}{\partial \mathbf{x}^2\partial \mathbf{y}^2} - 2(\mathbf{H}^s_{12}(\mathbf{x}) + 2\mathbf{H}^s_{66}(\mathbf{x}))\frac{\partial^4 \mathbf{w_s}}{\partial \mathbf{x}^2\partial \mathbf{y}^2} - 2\left(\mathbf{D}^{s'}_{12}(\mathbf{x}) + 2\mathbf{D}^{s'}_{66}(\mathbf{x})\right)\frac{\partial^3 \mathbf{w_b}}{\partial \mathbf{x}\partial \mathbf{y}^2} \\
& - \mathbf{H}^s_{11}(\mathbf{x})\frac{\partial^4 \mathbf{w_s}}{\partial \mathbf{x}^4} - \mathbf{H}^s_{22}(\mathbf{x})\frac{\partial^4 \mathbf{w_s}}{\partial \mathbf{y}^4} - 2\left(\mathbf{H}^{s'}_{12}(\mathbf{x}) + 2\mathbf{H}^{s'}_{66}(\mathbf{x})\right)\frac{\partial^3 \mathbf{w_s}}{\partial \mathbf{x}\partial \mathbf{y}^2} - 2\,\mathbf{D}^{s'}_{11}(\mathbf{x})\frac{\partial^3 \mathbf{w_b}}{\partial \mathbf{x}^3} - \mathbf{H}^{s'}_{11}(\mathbf{x})\frac{\partial^3 \mathbf{w_s}}{\partial \mathbf{x}^3} \\
& - \mathbf{D}^{s''}_{11}(\mathbf{x})\frac{\partial^2 \mathbf{w_b}}{\partial \mathbf{x}^2} - \mathbf{D}^{s''}_{12}(\mathbf{x})\frac{\partial^2 \mathbf{w_b}}{\partial \mathbf{y}^2} - \mathbf{H}^{s''}_{11}(\mathbf{x})\frac{\partial^2 \mathbf{w_s}}{\partial \mathbf{x}^2} - \mathbf{H}^{s''}_{12}(\mathbf{x})\frac{\partial^2 \mathbf{w_s}}{\partial \mathbf{y}^2} + \mathbf{A}^s_{44}(\mathbf{x})\frac{\partial^2 \mathbf{w_s}}{\partial \mathbf{y}^2} + \mathbf{A}^s_{55}(\mathbf{x})\frac{\partial^2 \mathbf{w_s}}{\partial \mathbf{x}^2} \\
& + \mathbf{A}^{s'}_{55}\frac{\partial \mathbf{w_s}}{\partial \mathbf{x}} + \bar{N}^0 + K_p\nabla^2(\mathbf{w_b} + \mathbf{w_s}) - K_w(\mathbf{w_b} + \mathbf{w_s}) = 0
\end{aligned} \tag{18}$$

Note that the superscripts $'$ and $''$ denote the first-and second derivatives with respect to x.

In buckling analysis, the plate is subjected to in-plane compressive loads of the following form:

$$N^0_x = \gamma_1 N_{cr}\,, \quad N^0_y = \gamma_2 N_{cr}\,, \; N^0_{xy} = 0 \tag{19.a}$$

where γ_1 and γ_2 are non-dimensional load parameters and N_{cr} is the critical buckling load.

Substituting Eq. (19.a) in Eq. (8.b) and considering N_{cr} as a compressive load, therefore:

$$\bar{N}^0 = -N_{cr}\left(\gamma_1 \frac{\partial^2 \bar{w}}{\partial x^2} + \gamma_2 \frac{\partial^2 \bar{w}}{\partial y^2}\right) \tag{19.b}$$

The types of buckling loads, (γ_1,γ_2) are (1, 0), (0, 1) and (1, 1). The used boundary conditions are:

$$\text{Clamped edge:}\quad w_b,\ w_s,\ u_{\bar{n}},\ u_{\bar{s}},\frac{\partial w_b}{\partial \bar{n}},\frac{\partial w_s}{\partial \bar{n}},\frac{\partial w_b}{\partial \bar{s}},\frac{\partial w_s}{\partial \bar{s}} \tag{20.a}$$

$$\text{Simply supported edge:}\quad w_b,\ w_s, u_{\bar{s}}, N_{\bar{n}\bar{n}}, M^b_{\bar{n}\bar{n}}, M^s_{\bar{n}\bar{n}} \tag{20.b}$$

$$\text{Free edge:}\quad N_{\bar{n}\bar{n}}, N_{\bar{n}\bar{s}}, M^b_{\bar{n}\bar{n}}, M^s_{\bar{n}\bar{n}}, V^b_{\bar{n}}, V^s_{\bar{n}} \tag{20.c}$$

where

$$u_{\bar{n}} = u_o\bar{n}_x + v_o\bar{n}_y \qquad u_{\bar{s}} = -u_o\bar{n}_y + v_o\bar{n}_x, \tag{20.d}$$

$$N_{\bar{n}\bar{n}} = N_x\bar{n}_x^2 + N_y\bar{n}_y^2 + 2N_{xy}\bar{n}_x\bar{n}_y \qquad N_{\bar{n}\bar{s}} = (N_y - N_x)\bar{n}_x\bar{n}_y + N_{xy}\left(\bar{n}_x^2 - \bar{n}_y^2\right) \tag{20.e}$$

$$M^b_{\bar{n}\bar{n}} = M^b_x\bar{n}_x^2 + M^b_y\bar{n}_y^2 + 2M^b_{xy}\bar{n}_x\bar{n}_y \qquad M^s_{\bar{n}\bar{n}} = M^s_x\bar{n}_x^2 + M^s_y\bar{n}_y^2 + 2M^s_{xy}\bar{n}_x\bar{n}_y \tag{20.f}$$

$$M^b_{\bar{n}\bar{s}} = (M^b_y - M^b_x)\bar{n}_x\bar{n}_y + M^b_{xy}(\bar{n}_x^2 - \bar{n}_y^2) \qquad M^s_{\bar{n}\bar{s}} = (M^s_y - M^s_x)\bar{n}_x\bar{n}_y + M^s_{xy}(\bar{n}_x^2 - \bar{n}_y^2), \tag{20.g}$$

$$Q^b_x = \frac{\partial M^b_x}{\partial x} + \frac{\partial M^b_{xy}}{\partial y} + N^o_x\frac{\partial(w_b+w_s)}{\partial x} + N^o_{xy}\frac{\partial(w_b+w_s)}{\partial y} \qquad Q^b_y = \frac{\partial M^b_{xy}}{\partial x} + \frac{\partial M^b_y}{\partial y} + N^o_{xy}\frac{\partial(w_b+w_s)}{\partial x} + N^o_y\frac{\partial(w_b+w_s)}{\partial y} \tag{20.h}$$

$$Q^s_x = \frac{\partial M^s_x}{\partial x} + \frac{\partial M^s_{xy}}{\partial y} + S^s_{xz} + N^o_x\frac{\partial(w_b+w_s)}{\partial x} + N^o_{xy}\frac{\partial(w_b+w_s)}{\partial y} \tag{20.i}$$

$$Q^s_y = \frac{\partial M^s_y}{\partial y} + \frac{\partial M^s_{xy}}{\partial x} + S^s_{yz} + N^o_y\frac{\partial(w_b+w_s)}{\partial y} + N^o_{xy}\frac{\partial(w_b+w_s)}{\partial x} \tag{20.j}$$

$$Q^b_{\bar{n}} = Q^b_x\bar{n}_x + Q^b_y\bar{n}_y \qquad Q^s_{\bar{n}} = Q^s_x\bar{n}_x + Q^s_y\bar{n}_y \tag{20.k}$$

$$V^b_{\bar{n}} = Q^b_{\bar{n}} + \frac{\partial M^b_{\bar{n}\bar{s}}}{\partial \bar{s}} \qquad V^s_{\bar{n}} = Q^s_{\bar{n}} + \frac{\partial M^s_{\bar{n}\bar{s}}}{\partial \bar{s}} \tag{20.l}$$

$$\frac{\partial w_i}{\partial \bar{n}} = \bar{n}_x\frac{\partial w_i}{\partial x} + \bar{n}_y\frac{\partial w_i}{\partial y} \qquad \frac{\partial w_i}{\partial \bar{s}} = \bar{n}_x\frac{\partial w_i}{\partial y} - \bar{n}_y\frac{\partial w_i}{\partial x} \tag{20.m}$$

where i refer to b or s, $\bar{n}$ and $\bar{s}$ are normal and tangent directions at a point having direction cosines $(\bar{n}_x$ and $\bar{n}_y)$ on a curved boundary.

3. Basic Idea of Differential/Integral Quadrature Method

The stress resultants included in Eq. (13) have been defined in Eq. (11) as functions of displacements $u_o(x,y)$, $v_o(x,y)$, $w_b(x,y)$, $w_s(x,y)$ and their derivatives with respect to (x,y). Furthermore, due to the assumption that the material properties change in the x-direction, the coefficients in these functions are dependent on the coordinate x. Such system of variable coefficients partial differential equations is very hard to be solved analytically. So, in this work, the efficient Differential/Integral Quadrature method (DIQM) is adopted and modified to solve this system. The mathematical fundamentals, recent developments and major applications of differential quadrature method (DQM) and DIQM in science and engineering can be found in [67-71].

3.1 Classical DQM for ordinary differential equations (1-D problems)

Let the domain $0 \le x \le a$ of the problem be discretized using n nodes; $x_1 = 0, x_2, ..., x_n = a$. To attain the DQM efficiency, these discrete nodes must be distributed according to the Chebyshev–Gauss–Lobatto formula [67]. Let the unknown function $\theta(x)$ be represented by the unknown vector $\theta = [\theta_1, \theta_2, ..., \theta_n]^T$ where $\theta_i = \theta(x_i)$. According to the DQM, the first order derivative of $\theta(x)$ at a given node, x_i, is approximated using a weighted sum of the values of $\theta_1, \theta_2, \cdots, \theta_n$ such that:

$$\left.\frac{d\theta}{dx}\right|_{x=x_i} \cong \sum_{j=1}^{n} d_{ij}\theta_j \ , \quad i = 1,2,\cdots,n \tag{21}$$

where d_{ij} denotes the corresponding weighting coefficients [68]. Equation (20) can be put in the matrix form as:

$$\bar{\boldsymbol{\theta}} = D\boldsymbol{\theta} \tag{22}$$

where vector $\bar{\boldsymbol{\theta}} = [\theta_1', \theta_2', ..., \theta_n']^T$, $\theta_i' = (d\theta / dx)_{x_i}$ is the DQM approximation of the first derivative $d\theta / dx$ and D is the first order weighting matrix of dimension $n \times n$ with typical elements d_{ij}. The DQM approximations of higher order derivatives can be obtained through matrix multiplication. For example, the second derivative $d^2\theta / dx^2$ and third order $d^3\theta / dx^3$ are approximated by DQM as $D^2\ \boldsymbol{\theta}$ and $D^3\ \boldsymbol{\theta}$, respectively.

3.2 DQM for a partial differential equation (2-D problem)

Consider a partial differential equation in the unknown function $\theta(x,y)$. The two-dimensional domain of the independent variables $0 < x < a$, $0 < y < b$ is discretized by n- and m-points, respectively. However, the objective of the discretization process is to transform the partial differential equation into an algebraic system in an unknown vector $\boldsymbol{\theta}$ consisting of all discrete values of the unknown function. For this purpose, the unknowns $\theta_{ij} = \theta(x_j, y_i),\ i = 1,\cdots,m, j = 1,\cdots,n$ defined on the rectangular domain are rearranged vector after vector to form the whole unknown vector:

$$\boldsymbol{\theta} = [\theta_{11}, \theta_{21}, \cdots \theta_{m1}, \theta_{12}, \theta_{22}, \cdots \theta_{m2}, \cdots, \cdots, \theta_{1n}, \theta_{2n}, \cdots \theta_{mn}]^T \tag{23}$$

Let D_x be the first order derivative matrix with respect to x of dimension $n \times n$ and let D_y be the first order derivative matrix with respect to y of dimension $m \times m$. To be consistent with the arrangement of unknowns given in Eq. (23) for vector $\boldsymbol{\theta}$, the Kronecker product is used to construct global derivative matrices of dimension $(mn \times mn)$ as:

$$\begin{Bmatrix} \mathbb{D}_x \\ \mathbb{D}_y \end{Bmatrix} = \begin{Bmatrix} D_x \otimes I_m \\ I_n \otimes D_y \end{Bmatrix} \tag{24}$$

where I_n and I_m are the identity matrices of dimensions $n \times n$ and $m \times m$, respectively and $\otimes$ denotes the Kronecker product. Based on Eq. (24), DQM can approximate higher and mixed partial derivatives such as $\partial^2\theta / \partial x^2$, $\partial^2\theta / \partial y^2$, $\partial^2\theta / \partial x\partial y$ by $\mathbb{D}_{xx}\ \boldsymbol{\theta}$, $\mathbb{D}_{yy}\ \boldsymbol{\theta}$ and $\mathbb{D}_{xy}\ \boldsymbol{\theta}$, respectively, where $\mathbb{D}_{xx} = \mathbb{D}_x^2$, $\mathbb{D}_{yy} = \mathbb{D}_y^2$, and $\mathbb{D}_{xy} = \mathbb{D}_x \mathbb{D}_y$.

3.3 DQM discretization of stress resultants and governing equations

As derived in Sec. 2, the modeling of BDFG unified plate results in a set of variable coefficients partial differential equations (Eq. (13)). To extend the application of DQM to solve such system we first consider a typical variable coefficient term $T(x,y) = A(x)\ \partial\theta / \partial y$. Since DQM approximates $\partial\theta / \partial y$ by the nm-vector $\mathbb{D}_y\ \boldsymbol{\theta}$ and to enable direct contribution of this term to the algebraic system, the variable coefficient $A(x)$ has to be properly discretized as nm-vector. The resulting nm-vector $\boldsymbol{\mathcal{A}}$ is used to approximate $A(x)\partial\theta / \partial y$ as follows:

$$\mathcal{A} \circ (\mathbb{D}_y\ \boldsymbol{\theta}) = (\mathcal{A} \circ \mathbb{D}_y)\ \boldsymbol{\theta} \tag{25}$$

The operator '$\circ$' in Eq. (25) is defined such that for a vector $\boldsymbol{\mathcal{V}}$ of dimensions $(n \times 1)$ and a matrix $\mathcal{M}$ of dimensions $(n \times m)$ (i.e. each of $\boldsymbol{\mathcal{V}}$ and $\mathcal{M}$ must have the same number of rows), $\boldsymbol{\mathcal{V}} \circ \mathcal{M} = \mathcal{Y}$, implies that $\mathcal{Y}$ is a $(n \times m)$-matrix such that $\mathcal{Y}_{ij} = \boldsymbol{\mathcal{V}}_i \circ \mathcal{M}_{ij}$.

Using these terminologies, stress resultants (Eq. (11)) can be discretized by DIQM as

$$\begin{bmatrix} \mathbf{N}_x \\ \mathbf{N}_y \\ \mathbf{N}_{xy} \\ \mathbf{M}_x^b \\ \mathbf{M}_y^b \\ \mathbf{M}_{xy}^b \\ \mathbf{M}_x^s \\ \mathbf{M}_y^s \\ \mathbf{M}_{xy}^s \end{bmatrix} = \begin{bmatrix} \mathcal{A}_{11} \circ \mathbb{D}_x & \mathcal{A}_{12} \circ \mathbb{D}_y & -(\mathcal{B}_{11} \circ \mathbb{D}_{xx} + \mathcal{B}_{12} \circ \mathbb{D}_{yy}) & -(\mathcal{B}_{11}^s \circ \mathbb{D}_{xx} + \mathcal{B}_{12}^s \circ \mathbb{D}_{yy}) \\ \mathcal{A}_{12} \circ \mathbb{D}_x & \mathcal{A}_{22} \circ \mathbb{D}_y & -(\mathcal{B}_{12} \circ \mathbb{D}_{xx} + \mathcal{B}_{22} \circ \mathbb{D}_{yy}) & -(\mathcal{B}_{12}^s \circ \mathbb{D}_{xx} + \mathcal{B}_{22}^s \circ \mathbb{D}_{yy}) \\ \mathcal{A}_{66} \circ \mathbb{D}_y & \mathcal{A}_{66} \circ \mathbb{D}_x & -2\mathcal{B}_{66} \circ \mathbb{D}_{xy} & -2\mathcal{B}_{66}^s \circ \mathbb{D}_{xy} \\ \mathcal{B}_{11} \circ \mathbb{D}_x & \mathcal{B}_{12} \circ \mathbb{D}_y & -(\mathcal{D}_{11} \circ \mathbb{D}_{xx} + \mathcal{D}_{12} \circ \mathbb{D}_{yy}) & -(\mathcal{D}_{11}^s \circ \mathbb{D}_{xx} + \mathcal{D}_{12}^s \circ \mathbb{D}_{yy}) \\ \mathcal{B}_{12} \circ \mathbb{D}_x & \mathcal{B}_{22} \circ \mathbb{D}_y & -(\mathcal{D}_{12} \circ \mathbb{D}_{xx} + \mathcal{D}_{22} \circ \mathbb{D}_{yy}) & -(\mathcal{D}_{12}^s \circ \mathbb{D}_{xx} + \mathcal{D}_{22}^s \circ \mathbb{D}_{yy}) \\ \mathcal{B}_{66} \circ \mathbb{D}_y & \mathcal{B}_{66} \circ \mathbb{D}_x & -2\mathcal{D}_{66} \circ \mathbb{D}_{xy} & -2\mathcal{D}_{66}^s \circ \mathbb{D}_{xy} \\ \mathcal{B}_{11}^s \circ \mathbb{D}_x & \mathcal{B}_{12}^s \circ \mathbb{D}_y & -(\mathcal{D}_{11}^s \circ \mathbb{D}_{xx} + \mathcal{D}_{12}^s \circ \mathbb{D}_{yy}) & -(\mathcal{H}_{11}^s \circ \mathbb{D}_{xx} + \mathcal{H}_{12}^s \circ \mathbb{D}_{yy}) \\ \mathcal{B}_{12}^s \circ \mathbb{D}_x & \mathcal{B}_{22}^s \circ \mathbb{D}_y & -(\mathcal{D}_{12}^s \circ \mathbb{D}_{xx} + \mathcal{D}_{22}^s \circ \mathbb{D}_{yy}) & -(\mathcal{H}_{12}^s \circ \mathbb{D}_{xx} + \mathcal{H}_{22}^s \circ \mathbb{D}_{yy}) \\ \mathcal{B}_{66}^s \circ \mathbb{D}_y & \mathcal{B}_{66}^s \circ \mathbb{D}_x & -2\mathcal{D}_{66}^s \circ \mathbb{D}_{xy} & -2\mathcal{H}_{66}^s \circ \mathbb{D}_{xy} \end{bmatrix} \begin{bmatrix} \mathbf{U} \\ \mathbf{V} \\ \mathbf{W}_b \\ \mathbf{W}_s \end{bmatrix} \tag{26.a}$$

$$\begin{bmatrix} \mathbf{S}_{yz}^s \\ \mathbf{S}_{xz}^s \end{bmatrix} = \begin{bmatrix} \mathcal{A}_{44}^s \circ \mathbb{D}y & 0 \\ 0 & \mathcal{A}_{55}^s \circ \mathbb{D}x \end{bmatrix} \begin{bmatrix} \mathbf{W}_s \\ \mathbf{W}_s \end{bmatrix} = \begin{bmatrix} \mathcal{A}_{44}^s \circ Dy \\ \mathcal{A}_{55}^s \circ Dx \end{bmatrix} \mathbf{W}_s \tag{26.b}$$

Now, since the mathematical model for the unified BDFG plate consists of four equations in the unknown functions $u_0(x,y)$, $v_0(x,y)$, $w_b(x,y)$, and $w_s(x,y)$, the overall discretized unknown vector is defined by $X = [\mathbf{U}^T, \mathbf{V}^T, \mathbf{W}_b^T, \mathbf{W}_s^T]^T$ where each of $\mathbf{U}, \mathbf{V}, \mathbf{W}_b, \mathbf{W}_s$ is $(nm \times 1)$ vector.

Finally, DQM discretization of Eq. (13) for buckling analysis can be put in the form of eigenvalue problem in the matrix form as:

$$(\mathcal{K} - N_{cr}\ \mathcal{N})\mathbf{X} = 0 \tag{27}$$

where

$$\mathcal{N} = \begin{bmatrix} \mathbb{O} & \mathbb{O} & \mathbb{O} & \mathbb{O} \\ \mathbb{O} & \mathbb{O} & \mathbb{O} & \mathbb{O} \\ \mathbb{O} & \mathbb{O} & (\gamma_1 \mathbb{D}_{xx} + \gamma_2 \mathbb{D}_{yy}) & (\gamma_1 \mathbb{D}_{xx} + \gamma_2 \mathbb{D}_{yy}) \\ \mathbb{O} & \mathbb{O} & (\gamma_1 \mathbb{D}_{xx} + \gamma_2 \mathbb{D}_{yy}) & (\gamma_1 \mathbb{D}_{xx} + \gamma_2 \mathbb{D}_{yy}) \end{bmatrix} \tag{28}$$

where $\mathbb{O}$ and $\mathbb{I}$ are the zero and identity matrices of dimensions $(mn \times mn)$, respectively. The elements of the stiffness $[\mathcal{K}]$ matric can be evaluated by:

$$K_{11} = \mathbb{D}x(\mathcal{A}_{11} \circ \mathbb{D}_x) + \mathbb{D}y(\mathcal{A}_{66} \circ \mathbb{D}_y) \qquad K_{12} = \mathbb{D}x(\ \mathcal{A}_{12} \circ \mathbb{D}_y) + \mathbb{D}y(\mathcal{A}_{66} \circ \mathbb{D}_x) \tag{29.a}$$

$$K_{13} = -\mathbb{D}x(\mathcal{B}_{11} \circ \mathbb{D}_{xx} + \mathcal{B}_{12} \circ \mathbb{D}_{yy}) - \mathbb{D}y(2\mathcal{B}_{66} \circ \mathbb{D}_{xy}) \tag{29.b}$$

$$K_{14} = -\mathbb{D}x(\mathcal{B}_{11}^{s} \circ \mathbb{D}_{xx} + \mathcal{B}_{12}^{s} \circ \mathbb{D}_{yy}) - \mathbb{D}y\left(2\mathcal{B}_{66}^{s} \circ \mathbb{D}_{xy}\right) \tag{29.c}$$

$$K_{21} = \mathbb{D}x\left(\mathcal{A}_{66} \circ \mathbb{D}_{y}\right) + \mathbb{D}y\left(\mathcal{A}_{12} \circ \mathbb{D}_{x}\right) \qquad K_{22} = \mathbb{D}x\left(\mathcal{A}_{66} \circ \mathbb{D}_{x}\right) + \mathbb{D}y\left(\mathcal{A}_{22} \circ \mathbb{D}_{y}\right) \tag{29.d}$$

$$K_{23} = -\mathbb{D}x\left(2\mathcal{B}_{66} \circ \mathbb{D}_{xy}\right) - \mathbb{D}y(\mathcal{B}_{12} \circ \mathbb{D}_{xx} + \mathcal{B}_{22} \circ \mathbb{D}_{yy}) \tag{29.e}$$

$$K_{24} = -\mathbb{D}x\left(2\mathcal{B}_{66}^{s} \circ \mathbb{D}_{xy}\right) - \mathbb{D}y(\mathcal{B}_{12}^{s} \circ \mathbb{D}_{xx} + \mathcal{B}_{22}^{s} \circ \mathbb{D}_{yy}) \tag{29.f}$$

$$K_{31} = \mathbb{D}xx\left(\mathcal{B}_{11} \circ \mathbb{D}_{x}\right) + 2\mathbb{D}xy\left(\mathcal{B}_{66} \circ \mathbb{D}_{y}\right) + \mathbb{D}yy\left(\mathcal{B}_{12} \circ \mathbb{D}_{x}\right) \tag{29.g}$$

$$K_{32} = \mathbb{D}xx\left(\mathcal{B}_{12} \circ \mathbb{D}_{y}\right) + 2\mathbb{D}xy\left(\mathcal{B}_{66} \circ \mathbb{D}_{x}\right) + \mathbb{D}yy\left(\mathcal{B}_{22} \circ \mathbb{D}_{y}\right) \tag{29.h}$$

$$K_{33} = -\mathbb{D}xx\left((\mathcal{D}_{11} \circ \mathbb{D}_{xx} + \mathcal{D}_{12} \circ \mathbb{D}_{yy})\right) - 2\mathbb{D}xy\left(2\mathcal{D}_{66} \circ \mathbb{D}_{xy}\right) - \mathbb{D}yy\left((\mathcal{D}_{12} \circ \mathbb{D}_{xx} + \mathcal{D}_{22} \circ \mathbb{D}_{yy})\right) + \left(K_{p}\left(\mathbb{D}xx + \mathbb{D}yy\right) - K_{w}\mathbb{I}\right) \tag{29.i}$$

$$K_{34} = \mathbb{D}xx\left(-(\mathcal{D}_{11}^{s} \circ \mathbb{D}_{xx} + \mathcal{D}_{12}^{s} \circ \mathbb{D}_{yy})\right) - 2\mathbb{D}xy\left(2\mathcal{D}_{66}^{s} \circ \mathbb{D}_{xy}\right) - \mathbb{D}yy\left((\mathcal{D}_{12}^{s} \circ \mathbb{D}_{xx} + \mathcal{D}_{22}^{s} \circ \mathbb{D}_{yy})\right) + \left(K_{p}\left(\mathbb{D}xx + \mathbb{D}yy\right) - K_{w}\mathbb{I}\right) \tag{29.j}$$

$$K_{41} = \mathbb{D}xx\left(\mathcal{B}_{11}^{s} \circ \mathbb{D}_{x}\right) + 2\mathbb{D}xy\left(\mathcal{B}_{66}^{s} \circ \mathbb{D}_{y}\right) + \mathbb{D}yy\left(\mathcal{B}_{12}^{s} \circ \mathbb{D}_{x}\right) \tag{29.k}$$

$$K_{42} = \mathbb{D}xx\left(\mathcal{B}_{12}^{s} \circ \mathbb{D}_{y}\right) + 2\mathbb{D}xy\left(\mathcal{B}_{66}^{s} \circ \mathbb{D}_{x}\right) + \mathbb{D}yy\left(\mathcal{B}_{22}^{s} \circ \mathbb{D}_{y}\right) \tag{29.l}$$

$$K_{43} = -\mathbb{D}xx\left(\mathcal{D}_{11}^{s} \circ \mathbb{D}_{xx} + \mathcal{D}_{12}^{s} \circ \mathbb{D}_{yy}\right) - 2\mathbb{D}xy\left(2\mathcal{D}_{66}^{s} \circ \mathbb{D}_{xy}\right) - \mathbb{D}yy\left((\mathcal{D}_{12}^{s} \circ \mathbb{D}_{xx} + \mathcal{D}_{22}^{s} \circ \mathbb{D}_{yy})\right) + \left(K_{p}\left(\mathbb{D}xx + \mathbb{D}yy\right) - K_{w}\mathbb{I}\right) \tag{29.m}$$

$$K_{44} = -\mathbb{D}xx\left(\mathcal{H}_{11}^{s} \circ \mathbb{D}_{xx} + \mathcal{H}_{12}^{s} \circ \mathbb{D}_{yy}\right) - 2\mathbb{D}xy\left(2\mathcal{H}_{66}^{s} \circ \mathbb{D}_{xy}\right) - \mathbb{D}yy\left(\mathcal{H}_{12}^{s} \circ \mathbb{D}_{xx} + \mathcal{H}_{22}^{s} \circ \mathbb{D}_{yy}\right) + \mathbb{D}x\left(\mathcal{A}_{55}^{s} \circ \mathbb{D}y\right) + \mathbb{D}y\left(\mathcal{A}_{44}^{s} \circ \mathbb{D}y\right) + \left(K_{p}\left(\mathbb{D}xx + \mathbb{D}yy\right) - K_{w}\mathbb{I}\right) \tag{29.n}$$

4. Numerical Results

This section is divided into two main subsections. The first one presents the validation of the present model with many previous peer works. The second subsection illustrates parametric studies to present the influence of no of nodes of DQM on the solution conversion, effects of shear functions, buckling load types, boundary conditions, gradation indices, porosity types, and elastic foundation on the critical buckling loads (eigenvalues) and associated mode shapes (eigenvectors) of bi-directional functionally graded porous unified plate. The material properties for metal and ceramic ingredients used through the analysis are presented in Table 2, and the notation for boundary conditions of plate are illustrated in Fig. 2.

4.1 Model Validations

Table 3 illustrates a comparison of uniaxial critical buckling load $\bar{N} = N_{cr}a^2/(E_m h^3)$ between the obtained results with different shear functions and results of Sadgui and Tati [46] and Thai and Choi [72] for isotropic Al/Al_2O_3 SSSS square plates with the following parameters $(h=1, a/h=10, n_x=0, \gamma_1=1, \gamma_2=0)$. As shown, the obtain results of Reddy, Thai and Kim, and Taibi shear functions are approximately identical with the results of Thai and Choi (2012) at different values of gradation index through thickness direction (n_z) and deviated by 0.1% from the results of Sadgui and Tati [64]. It is found that the buckling load in case of Karama shear function is higher than the other shear functions and less than the buckling obtained by Sadgui and Tati [46].

To validate the porosity models, the obtained buckling load for SSSS porous plate under uniaxial load vs gradation index through the thickness direction is compared with [65] at the same conditions, as shown in Fig. 3. It is found that the current porosity model is accurate and identical with the results obtained previously by [37]. As presented, the buckling load decreases exponentially with increasing of the gradation index and the buckling load for nonporous is higher than the two porosity models (Type 1 and Type 3).

Table 2. Material properties of BDFGM plate

Property/ Material	Metal			Ceramic			
	Aluminum (Al)	Stainless Steel (Sus_3O_4)	Ref. [54]	Alumina (Al_2O_3)	Silicon Nitride (Si_3N_4)	Silicon Carbide (SiC)	Ref. [54]
E (GPa)	70	201.04	1.44	380	348.43	420	14.4
ν	0.3	0.24	0.38	0.3	0.3	0.3	0.3
ρ (kg/m^3)	2707	2370	1220	3800	8166	3800	12200

Table 3. Comparison of the critical uniaxial buckling load $\bar{N} = N_{cr}a^2/(E_m h^3)$ of isotropic Al/Al_2O_3 SSSS square plates $(h = 1, a/h = 10, n_x = 0, \gamma_1 = 1, \gamma_2 = 0)$

Shear function		n_z			
		0	1	4	10
Touratier	Present	18.5801	9.3398	6.2371	5.4541
Karama		18.5849	9.3418	6.2357	5.4546
Reddy		18.5785	9.3391	6.2399	5.4553
Thai & Kim		18.5785	9.3391	6.2399	5.4553
Taibi		18.5793	9.3395	6.2432	5.4574
	Ref. [46]	**18.6015**	**9.3508**	**6.1961**	**5.41**
	Ref. [72]	**18.5785**	**9.3391**	**–**	**5.4528**

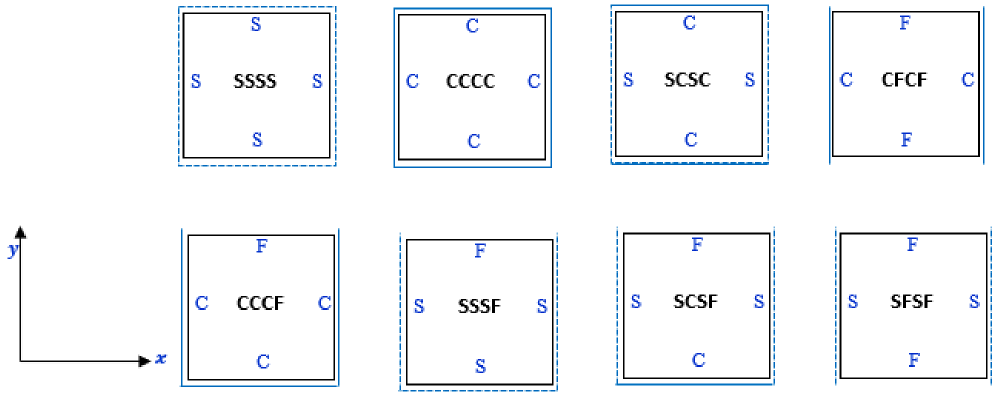

Fig. 2. The notation for plate boundary conditions

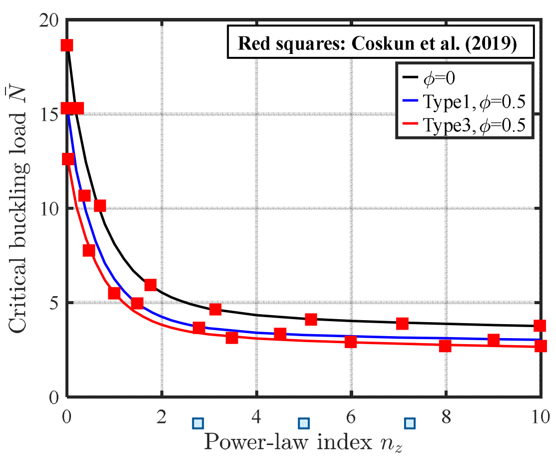

Fig. 3. Comparison of critical buckling load $\bar{N} = Na^2/E_m h^3$ of SSSS plate at different TFG indices and different porosity types with [50]

Table 4 validates the effect of elastic foundation influence on the buckling load of unidirectional FG SSSS square plates. As predicated, the current results are very close to the results obtained by Thai and Kim 2013) for all values of gradations and elastic parameters and deviate with 0.2% as maximum from the results obtained by Vu et al. (2021). It is found that, the critical buckling load for uniaxial is higher than that for biaxial load under the same boundary and geometrical conditions.

4.2 Parametric analysis

i. Convergence study

As we used a differential quadrature method in solving the proposed model, therefore, we should check the convergence of solution according to the number of discretization points for various boundary conditions (see Table 5 and Fig. 4). As concluded, the fully clamped and fully simply supported are convergent at any no of discrete points (i.e., ranging from 8 to 20 the deviation in results around 0.8% for CCCC and 0.9% for SSSS). However, the CCCF and CFCF boundary conditions are very sensitive to the no. of discrete points. The deviation for these two cases may around 9% and 6% respectively, as the no. of points increased from 8 to 20. It is found that for lower number of discrete points, the critical buckling load is underestimate for SCSC and overestimate for CCCF boundary conditions. It is also noted, the buckling loads for all boundary conditions are convergent after $N_{DQ} \geq 14$. Therefore, in the next analysis, we used $N_{DQ} = 15$ to confirm the convergence of the solution of buckling loads.

Table 4. The critical buckling load $\bar{N} = Na^2 / (E_m h^3)$ of isotropic Al / Al_2O_3 SSSS plates at $K_w = k_w a^4 / (E_m h^3 / 12(1-\nu^2))$, $K_p = k_p a^2 / (E_m h^3 / 12(1-\nu^2))$, $a / h = 5, b = a, h = 17.6\mu m, n_x = 0$

	(K_w, K_p)		n_z 0.5	1	2	5
Touratier	(100,10)	Uni-axial	13.3701	10.9866	9.1019	7.3315
Karama			13.3794	10.9936	9.1052	7.3258
Reddy			13.3664	10.9839	9.1025	7.3470
Thai&Kim			13.3664	10.9839	9.1025	7.3470
Taibi			13.3670	10.9845	9.1056	7.3666
Ref. [34]			13.3519	10.9793	9.1599	7.7612
Ref. [65]			13.3847	10.9838	9.1025	7.3459
Touratier	(1000,100)		27.0872	24.1630	21.6871	18.7675
Karama			27.1148	24.1843	21.6983	18.7679
Reddy			27.0740	24.1530	21.6858	18.7860
Thai&Kim			27.0740	24.1530	21.6858	18.7860
Taibi			27.0729	24.1525	21.6914	18.8143
Ref. [34]			26.5837	23.8605	21.6016	19.1802
Ref. [65]			27.0943	24.1530	21.6857	18.7837
Touratier	(100,10)	Bi-axial	6.6851	5.4933	4.5510	3.9022
Karama			6.6897	5.4968	4.5526	3.9001
Reddy			6.6832	5.4919	4.5513	3.9064
Thai&Kim			6.6832	5.4919	4.5513	3.9064
Taibi			6.6835	5.4923	4.5528	3.9114
Ref. [34]			6.5705	5.4131	4.5106	3.9272
Ref. [65]			6.6924	5.4919	4.5513	3.9062
Touratier	(1000,100)		19.1021	17.9104	16.9681	15.7770
Karama			19.1068	17.9139	16.9697	15.7725
Reddy			19.1003	17.9090	16.9683	15.7895
Thai&Kim			19.1003	17.9090	16.9683	15.7895
Taibi			19.1006	17.9093	16.9699	15.8052
Ref. [34]			18.7865	17.6719	16.8016	15.8832
Ref. [65]			19.1094	17.909	16.9683	15.7886

Table 5. Convergence of DQM of the critical buckling load ($\bar{N} = Na^2 / E_m h^3$) for Al / Al_2O_3 FG square plate under compression along x-direction for various boundary conditions

BCs	N_{DQ} 8	10	12	14	16	18	20
CCCC	15.4318	15.3823	15.3242	15.3156	15.3107	15.3072	15.3059
SCSC	10.1383	10.5447	10.5900	10.5868	10.5861	10.5855	10.5857
CCCF	7.9558	7.5360	7.3375	7.2678	7.2497	7.2229	7.2164
CFCF	6.5707	6.3463	6.2283	6.1845	6.1763	6.1663	6.1663
SSSS	6.2108	6.2577	6.2666	6.2668	6.2668	6.2669	6.2669
SCSF	2.7527	2.6965	2.6937	2.6942	2.6948	2.6947	2.6946
SSSF	2.3156	2.2923	2.2911	2.2914	2.2916	2.2918	2.2918
SFSF	1.5915	1.5740	1.5784	1.5726	1.5727	1.5728	1.5729

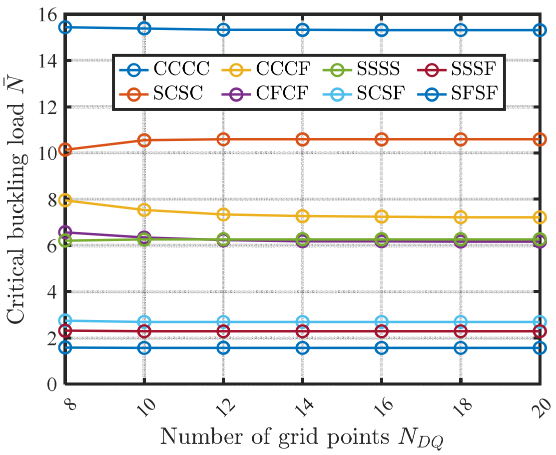

Fig. 4. Convergence of DQM of the critical buckling load ($\bar{N}$) for Al / Al_2O_3 BDFG square plate under compression along x-direction with different boundary conditions $n_x = n_z = 1; a / h = 20$

Table 6. DQM Comparison of the critical buckling $\bar{N} = Na^2 / E_m h^3$ of isotropic Al / Al_2O_3 SSSS square plates

Shear functions	Type of loading	a / h		
		5	10	20
Touratier	$\gamma_1 = 1, \gamma_2 = 0$	4.9039	5.9709	6.2669
Karama		4.9132	5.9729	6.2674
Reddy		4.8991	5.9702	6.2668
Thai & Kim		4.8991	5.9702	6.2668
Taibi		4.8983	5.9705	6.2669
Touratier	$\gamma_1 = 1, \gamma_2 = 1$	2.6779	3.1080	3.2358
Karama		2.6807	3.1088	3.2360
Reddy		2.6767	3.1077	3.2358
Thai & Kim		2.6767	3.1077	3.2358
Taibi		2.6769	3.1078	3.2358
Touratier	$\gamma_1 = 1, \gamma_2 = -1$	7.0210	10.8286	12.1683
Karama		7.0683	10.8377	12.1707
Reddy		6.9882	10.8249	12.1675
Thai & Kim		6.9882	10.8249	12.1675
Taibi		6.9716	10.8256	12.1679

Table 7. DQM Comparison of the critical uniaxial buckling $\bar{N} = Na^2 / E_m h^3$ of isotropic Al / Al_2O_3 square plates ($b = a = 1, n_x = 1, \gamma_1 = 1, \gamma_2 = 0$)

	BC	n_z				
		0	0.5	1	2	5
Touratier	**CCCC**	22.4997	17.4882	15.3166	13.5987	12.2980
Karama		22.5056	17.4922	15.3201	13.6008	12.2986
Reddy		22.4975	17.4866	15.3156	13.5989	12.2998
Thai & Kim		22.4974	17.4863	15.3157	13.5988	12.2999
Taibi		22.4983	17.4868	15.3160	13.6002	12.3027
Touratier	**SCSC**	14.5215	11.7489	10.5875	9.6758	8.9378
Karama		14.5252	11.7514	10.5897	9.6775	8.9389
Reddy		14.5202	11.7480	10.5868	9.6756	8.9382
Thai & Kim		14.5202	11.7480	10.5868	9.6756	8.9382
Taibi		14.5208	11.7484	10.5871	9.6763	8.9395
Touratier	**CCCF**	11.1236	8.4346	7.2668	6.3632	5.7378
Karama		11.1250	8.4299	7.2673	6.3604	5.7371
Reddy		11.1243	8.4264	7.2678	6.3635	5.7372
Thai & Kim		11.1222	8.4272	7.2702	6.3616	5.7371
Taibi		11.1224	8.4311	7.2656	6.3613	5.7387
Touratier	**CFCF**	9.4702	7.1836	6.1884	5.4147	4.8825
Karama		9.4730	7.1804	6.1891	5.4154	4.8822
Reddy		9.4699	7.1798	6.1845	5.4138	4.8830
Thai & Kim		9.4694	7.1835	6.1865	5.4156	4.8823
Taibi		9.4685	7.1840	6.1882	5.4141	4.8836
Touratier	**SSSS**	9.2917	7.1761	6.2669	5.5552	5.0439
Karama		9.2927	7.1768	6.2674	5.5555	5.0440
Reddy		9.2913	7.1759	6.2668	5.5552	5.0442
Thai & Kim		9.2913	7.1759	6.2668	5.5552	5.0442
Taibi		9.2915	7.1760	6.2669	5.5554	5.0445
Touratier	**SCSF**	4.2244	3.1459	2.6941	2.3533	2.1232
Karama		4.2246	3.1460	2.6942	2.3534	2.1232
Reddy		4.2243	3.1458	2.6942	2.3533	2.1233
Thai & Kim		4.2243	3.1458	2.6942	2.3533	2.1233
Taibi		4.2244	3.1458	2.6943	2.3534	2.1234
Touratier	**SSSF**	3.6034	2.6778	2.2914	2.0008	1.8052
Karama		3.6035	2.6779	2.2915	2.0009	1.8052
Reddy		3.6033	2.6777	2.2914	2.0008	1.8053
Thai & Kim		3.6033	2.6777	2.2914	2.0008	1.8053
Taibi		3.6034	2.6777	2.2914	2.0009	1.8053
Touratier	**SFSF**	2.4888	1.8404	1.5726	1.3739	1.2387
Karama		2.4889	1.8396	1.5726	1.3739	1.2387
Reddy		2.4888	1.8394	1.5726	1.3739	1.2387
Thai & Kim		2.4888	1.8397	1.5725	1.3746	1.2387
Taibi		2.4888	1.8395	1.5729	1.3740	1.2388

ii. Effect of uni/bi-directional loading and shear functions

In the current analysis, uniaxial (x-direction) at $\gamma_1 = 1, \gamma_2 = 0$, uniaxial (y-direction) at $\gamma_1 = 0, \gamma_2 = 1$, biaxial compression occurs at $\gamma_1 = \gamma_2 = 1$, and biaxial compression-tension by $\gamma_1 = 1$, $\gamma_2 = -1$. Table 6 presents comparison of critical buckling load, N_{cr} using transverse shear shape functions, $F(z)$ in Table 1 for a simply supported perfect square plate ($n_x = n_z = 1, \gamma_1 = 1, \gamma_2 = 0$) vs a/h . As concluded from Table 6, the lowest critical buckling load is noticed under bidirectional compression loads and highest critical buckling loads is observed for biaxial compression-tension loads which are compatible with a physical explanation (i.e., the stiffening of structure by a tension load). As shown, by increasing the ratio a/h the plate becomes stiffer and hence, the critical buckling loads increased. Based on shear functions, the obtained results for Reddy, Thai and Kim, and Taibi are approximately equal, however, Karama shear functions has the highest critical buckling load than the others.

iii. Effect of boundary conditions

Table 7 illustrates dimensionless critical uniaxial buckling load, N_{cr} versus boundary conditions and graduation index, n_z at $\phi = 0$, $b/a = 1$, $a/h = 20$, $n_x = 1$, without elastic foundation. It is observed that the maximum critical buckling load is noticed in case of fully clamped boundary condition, and the minimum critical buckling load is observed in case of SFSF boundary condition. By increasing the gradation parameter through the thickness direction, the buckling load is decreased significantly due to the changing of constituent from ceramic phase with higher Young modulus to metal phase with lower Young modulus, at the same other geometrical and boundary conditions. For example, in case of CCCC, the critical buckling load decreased by around 50% as n_z changed from 0 to 5. Removing the constraint from one side of CCCC/SSSS boundary conditions to free (CCCF/ SSSF), the critical buckling load is reduced by around 50-60%. Therefore, the boundary conditions have significant impact on the critical buckling load of bi-directional FG plates. The qualitative presentation of Table 7 for all boundary conditions with adding porosity and elastic foundation parameters is shown in Figure 5. Figure 6 illustrates the influence of gradation index through the axial direction on the 1st mode shape of BDFG plate versus different boundary conditions. As shown from this figure, the gradation index through the axial direction n_x tends to change the amplitude of mode shape rather than change in the geometrical shape. The gradation index is more significant for both CCCC and SFSF rather than the other boundary conditions.

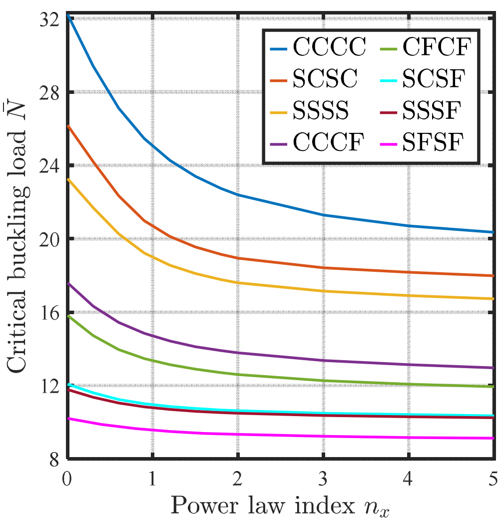

a) $n_z = 1$

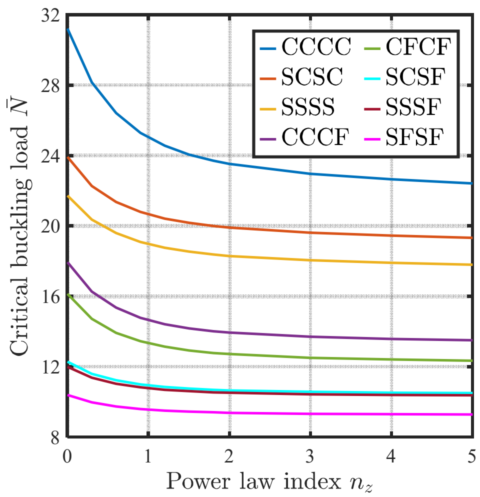

b) $n_x = 1$

Fig. 5. Dimensionless critical buckling load, N_{cr} of a square plate against four types of buckling loads, gradation indexes, n_z and n_x at all types of boundary conditions ($\gamma_1 = 1, \gamma_2 = 0$, $\phi = 0.5$, $b/a = 1$, $a/h = 20$, $K_w = 100$, and $K_p = 100$)

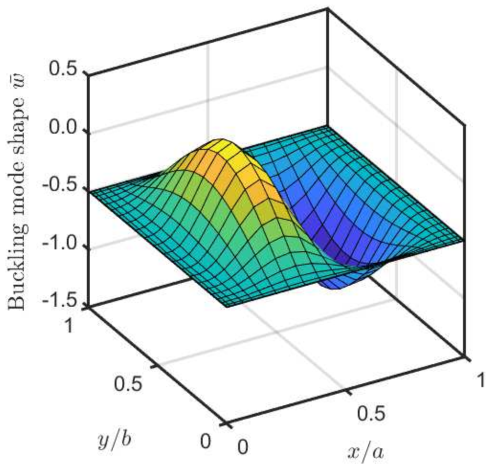

$n_x = 0$, $n_z = 5$, CCCC

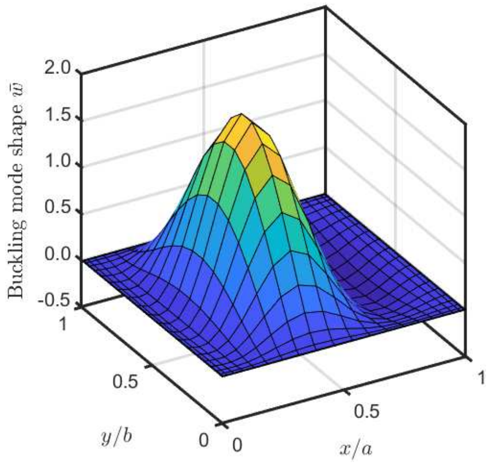

$n_x = 5$, $n_z = 5$, CCCC

Fig. 6. First buckling mode shapes, N_{cr} of square Al/Al_2O_3 plates ($a/h = 5, \gamma_1 = 1, \gamma_2 = 0$) versus boundary conditions

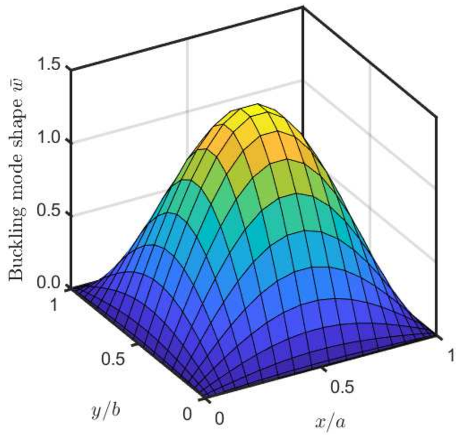

$n_x = 0$, $n_z = 5$, SSSS

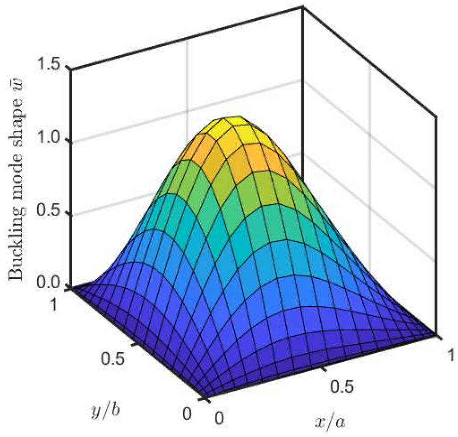

$n_x = 5$, $n_z = 5$, SSSS

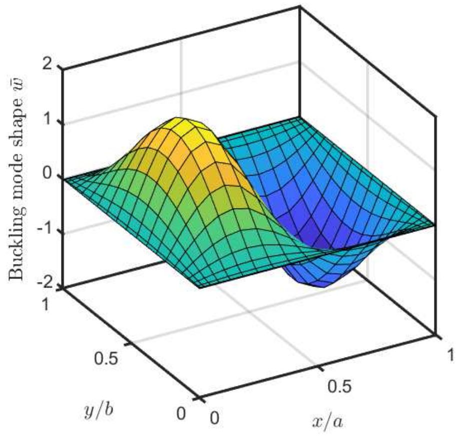

$n_x = 0$, $n_z = 5$, SCSC

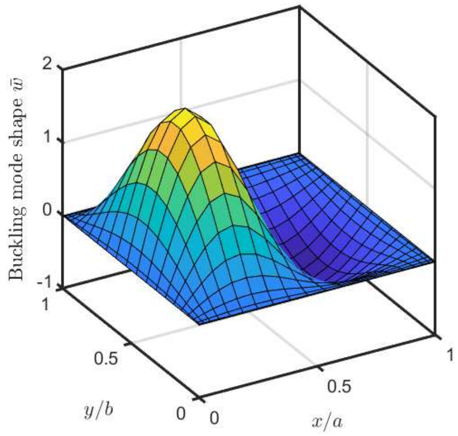

$n_x = 5$, $n_z = 5$, SCSC

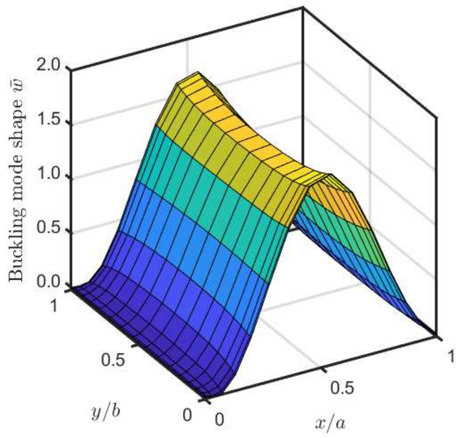

$n_x = 0$, $n_z = 5$, CFCF

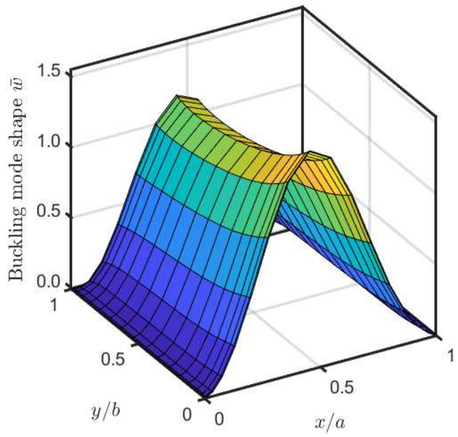

$n_x = 5$, $n_z = 5$, CFCF

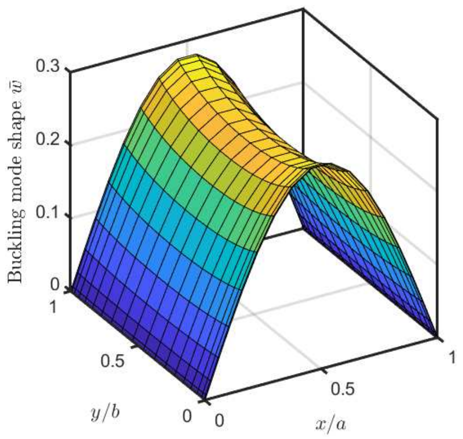

$n_x = 0$, $n_z = 5$, SFSF

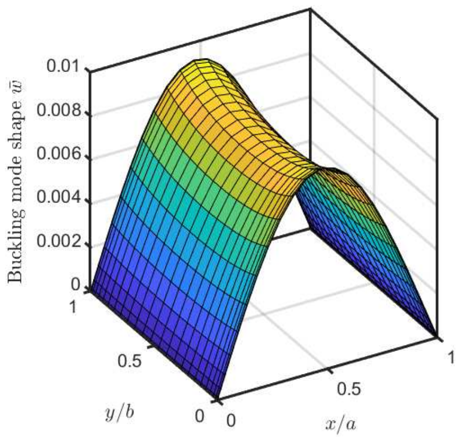

$n_x = 5$, $n_z = 5$, SFSF

Fig. 6. Continued

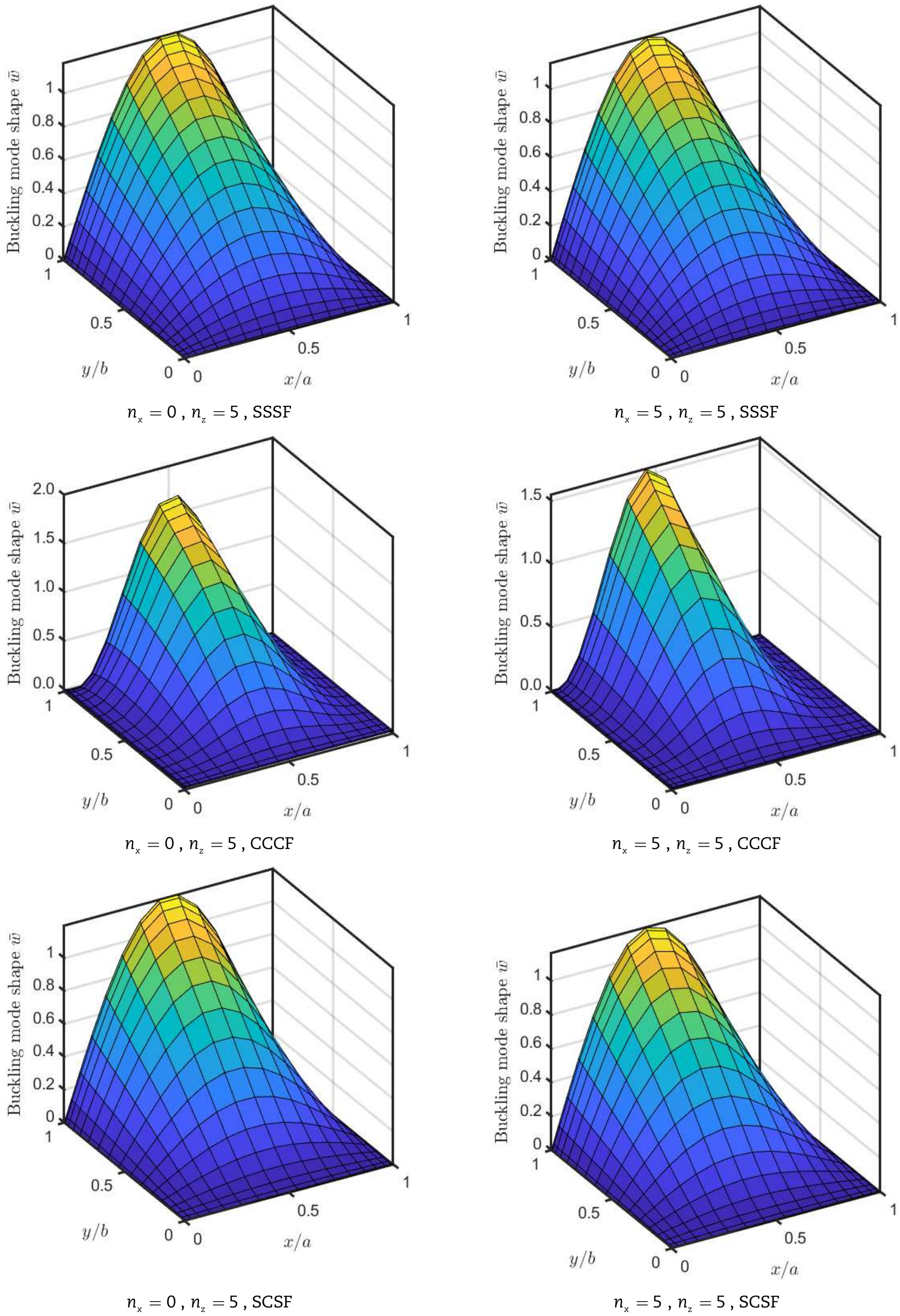

Fig. 6. Continued

iv. <u>Effect of gradation indices and geometrical dimensions</u>

Dimensionless critical uniaxial buckling load, N_{cr} of a clamped BDFG plate against gradation indices n_z and n_x, side to thickness ratio, (a/h) and plate aspect ratio (b/a) without elastic foundations and porosity is presented in Fig. 7. As shown in Figs. 7a and 7b, by increasing side to thickness ratio (a/h) the plate becomes thinner and stiffener therefore, the critical buckling load increased. The impact of plate aspect ratio (b/a) on the critical buckling load is presented in Figs. 7c and 7d. As shown, by increasing the aspect ratio (b/a), the geometry of plate changes from square plate (at $b/a = 1$) to rectangle plate (at $b/a \neq 1$) and the plate becomes less stiff, therefore the critical buckling load is decreased. It is also noted that, by increasing the gradation indices in x-direction n_x or z-direction n_z the critical buckling load decreased exponentially due to the softening in the plate (increasing the phase of metal material relative to the phase of ceramic). The gradation index through x-direction is more pronounce than the gradation in z-direction as depicted in Figs. 7a vs 7b or Figs. 7c vs 7d.

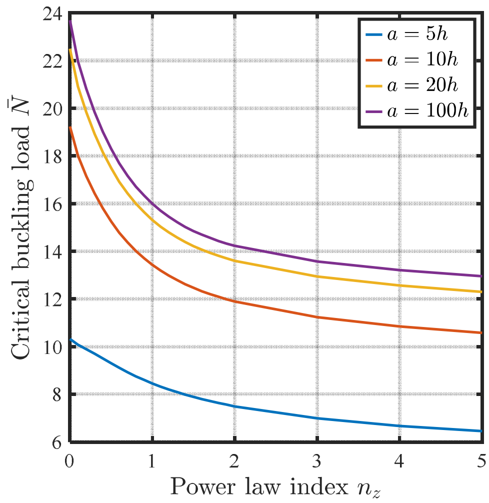

a) Buckling load ($\bar{N}$) versus gradation index n_z
(at $n_x = 1, b/a = 1$ and $\gamma_1 = 1, \gamma_2 = 0$)

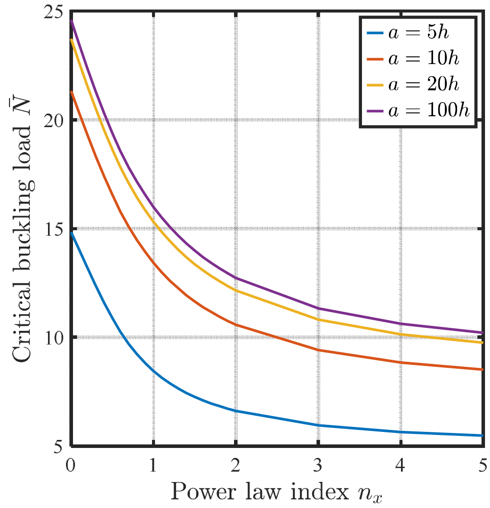

b) Buckling load ($\bar{N}$) versus gradation index n_x
(at $n_z = 1, b/a = 1$ and $\gamma_1 = 1, \gamma_2 = 0$)

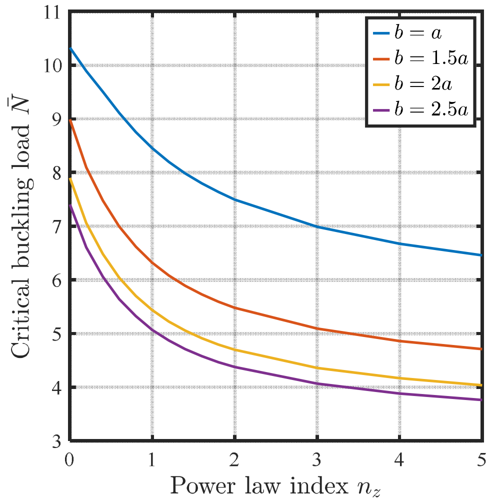

c) Buckling load ($\bar{N}$) versus gradation index n_z
(at $n_x = 1, a/h = 5$ and $\gamma_1 = 1, \gamma_2 = 0$)

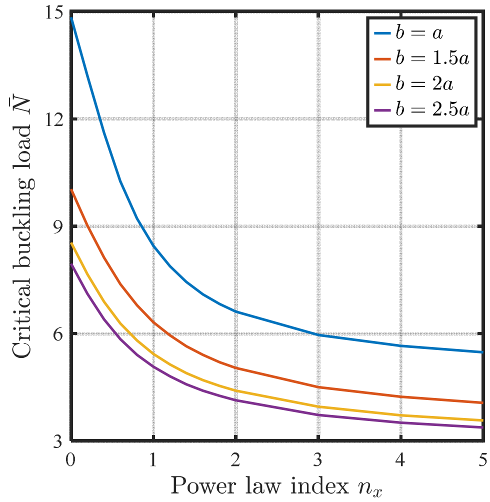

d) Buckling load ($\bar{N}$) versus gradation index n_x
(at $n_z = 1, a/h = 5$ and $\gamma_1 = 1, \gamma_2 = 0$)

Fig. 7. The effect of the gradient indices n_x and n_z on the dimensionless critical uniaxial buckling load $\bar{N} = Na^2 / E_m h^3$ of BDFG CCCC plate

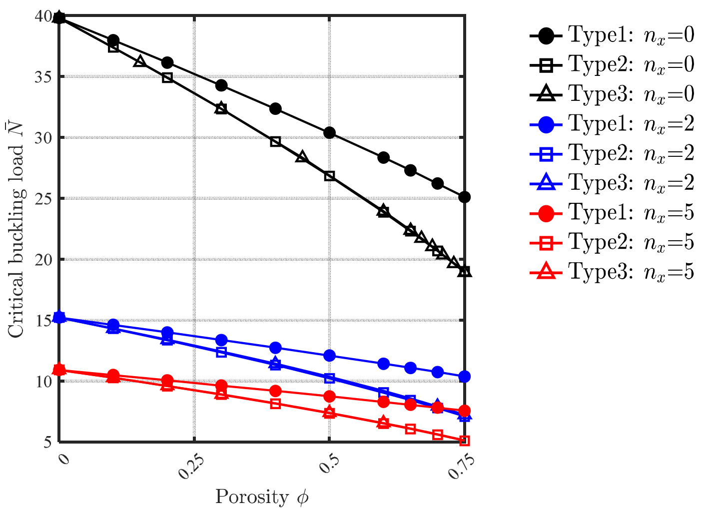

Fig. 8. Dimensionless critical uniaxial buckling load ($\bar{N}$) of CCCC plate at different gradient indices n_x and different porosity types at $n_z = 1$, $b/a = 1$, $a/h = 20$

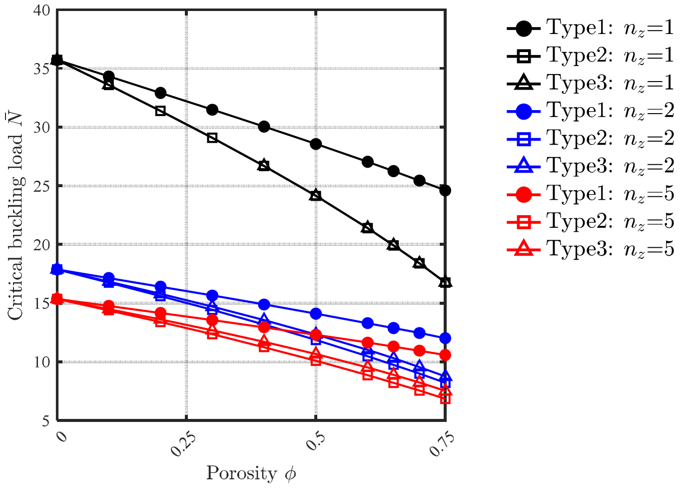

Fig. 9. Dimensionless critical uniaxial buckling load ($\bar{N}$) of CCCC plate at different gradient indices n_z and different porosity types at $n_x = 1$, $b/a = 1$, $a/h = 20$

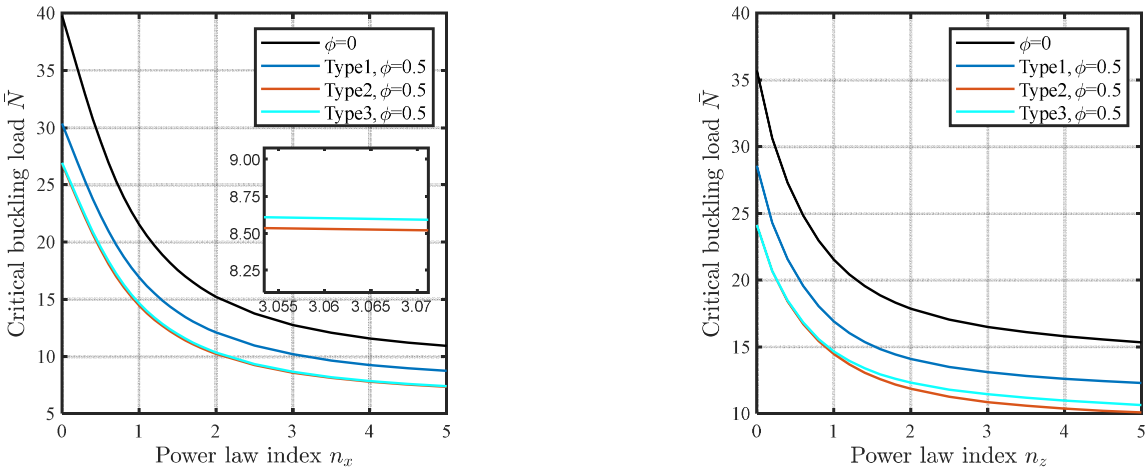

a) $n_z = 1$ b) $n_x = 1$

Fig. 10. Dimensionless critical uniaxial buckling load ($\bar{N}$) of CCCC plate at different gradient indices n_x and n_z for different porosity types ($b/a = 1$, $a/h = 20$)

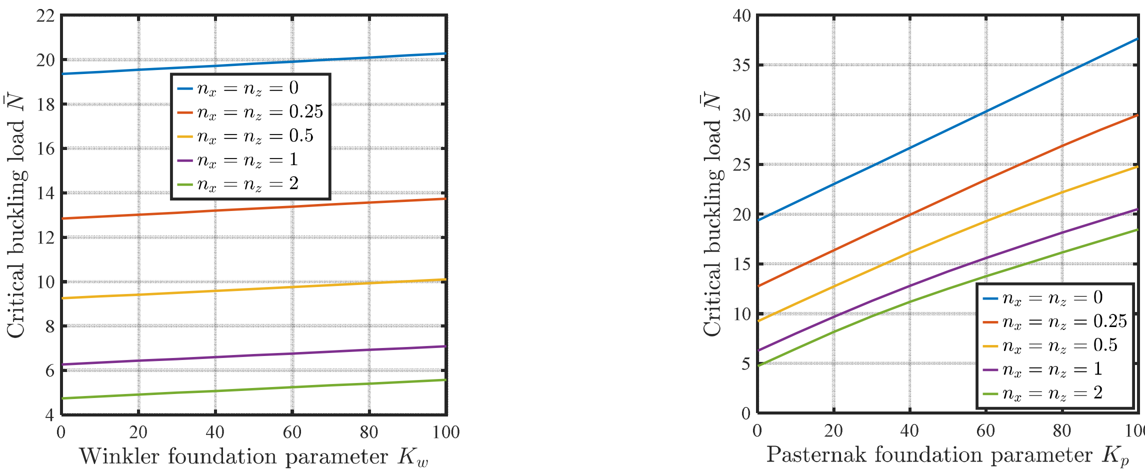

a) $K_p = 0$, $b/a = 1$, $a/h = 20$ b) $K_w = 0$, $b/a = 1$, $a/h = 20$

Fig. 11. Dimensionless critical uniaxial buckling load, N_{cr} of a perfect simply supported square plate against gradation indexes, n_x and n_z, and elastic foundation parameters, K_w and K_p

v. Effect of porosity types

Figures 8 and 9 present a critical uniaxial buckling load, N_{cr} of a clamped square plate vs porosity coefficient with different porosity types and various gradation indices n_x and n_z, respectively, at $b/a=1, a/h=20$. As shown from these figures, by increasing the internal void (porosity parameter), the material stiffness is decreased and hence the critical buckling load is reduced linearly. As predicted, the porosity types 2 and 3 are most significant on the softening of the material rather than the Type 1 (see Figs. 8-10). For a case in hand at $n_x=0$, the reduction in buckling for porosity Type 1 around 37% as the porosity parameter increased from 0 to 0.75. However, at the same conditions, the reduction in buckling is around 50% for porosity Types 2 and 3. By increasing the gradation index, the critical buckling is reduced.

vi. Effect of elastic foundations

The influences of elastic foundation parameters K_w and K_P on the critical buckling load of BDFG plate with SSSS boundary conditions are presented in Fig. 11. As predicted, the critical buckling load is increased linearly by increasing both elastic foundation parameters K_w and K_P. However, it is noticed that effect of K_P is more significant than the effect of K_w on the buckling load. In our case at $n_z=n_x=2$, by increasing the elastic foundation parameter K_P from 0 to 100, the buckling load is increased from 5 to 18 (increased by around 260%). However, if the elastic foundation parameter K_w increased from 0 to 100, the buckling load is increased from 4.6 to 5.8 (increased by 26%). Therefore, it can be concluded that the effect of K_P is ten times the effect of K_w on the critical buckling loads.

5. Conclusions

Through this study, the mathematical model for buckling analysis of bi-directional FG porous plate resting on elastic foundation was developed. Bi-directional gradation through axial and transverse directions was portrayed by power function distribution with three porosity types. Unified equivalent single layer theories of plate were used to describe the kinematic fields and without the necessity of shear correction factor. The governing equilibrium equations of BDFGPUP including the higher terms of force resultants and an efficient numerical approach named DIQM was exploited to solve the problem. The main points drawn from the parametric studies can be summarized as:

- For convergence analysis, the buckling loads for all boundary conditions are convergent after $\mathbf{N}_{\mathbf{DQ}} \geq 14$.
- The lowest critical buckling load is noticed under bidirectional compression loads and highest critical buckling loads is observed for biaxial compression-tension loads which are compatible with a physical explanation (i.e., the stiffening of structure by a tension load).
- In the case of CCCC boundary conditions, the critical buckling load decreased by around 50% as n_z changed from 0 to 5.
- Removing the constraint from one side of CCCC/SSSS boundary conditions to free (CCCF/ SSSF) ones, the critical buckling load is reduced by around 50-60%.
- By increasing the aspect ratio (*b/a*), the plate becomes less stiff, therefore the critical buckling load is decreased.
- By increasing the gradation indices in x-direction (n_x) or z-direction (n_z) the critical buckling load decreased exponentially due to the softening in the plate.
- The gradation index through the axial direction n_x tends to change the amplitude of mode shape rather than change in the geometrical shape
- By increasing the internal void (porosity parameter), the material stiffness is decreased and hence the critical buckling load is reduced linearly.
- The porosity patterns of types 2 and 3 are most significant on the softening of the material rather than that of type 1.
- The effect of K_P on the critical buckling loads is ten times higher than that of K_w.

Author Contributions

A.E. Assie planned the scheme, initiated the project, and suggested the parametric analyses; S.A. Mohamed and R.A. Shanab conducted the solution procedure and analyzed the empirical results; A.E. Assie and M.A. Eltaher developed the mathematical modeling. R.M. Abo-bakr examined the theory validation. The manuscript was written through the contribution of all authors. All authors discussed the results, reviewed, and approved the final version of the manuscript.

Acknowledgments

Not applicable.

Conflict of Interest

The authors declared no potential conflicts of interest concerning the research, authorship, and publication of this article.

Funding

The authors received no financial support for the research, authorship, and publication of this article.

Data Availability Statements

The datasets generated and/or analyzed during the current study are available from the corresponding author on reasonable request.

References

[1] Hassan, A.H, Kurgan, N., Can, N., The Relations between the Various Critical Temperatures of Thin FGM Plates, *Journal of Applied and Computational Mechanics*, 6, 2020, 1404-1419.

[2] Dorduncu, M., Olmus, I., Rabczuk, T., A peridynamic approach for modeling of two dimensional functionally graded plates, *Composite Structures*, 279, 2022, 114743.

[3] Alshorbagy, A.E., Eltaher, M.A., Mahmoud, F., Free vibration characteristics of a functionally graded beam by finite element method, *Applied*

Mathematical Modelling, 35(1), 2011, 412-425.
[4] Esen, I., Özarpa, C., Eltaher, M.A., Free vibration of a cracked FG microbeam embedded in an elastic matrix and exposed to magnetic field in a thermal environment, *Composite Structures*, 261, 2021, 113552.
[5] Shanab, R.A., Attia, M.A., Semi-analytical solutions for static and dynamic responses of bi-directional functionally graded nonuniform nanobeams with surface energy effect, *Engineering with Computers*, 2020, 1-44. DOI: 10.1007/s00366-020-01205-6
[6] Wu, C.P., Huang, H.Y., A semianalytical finite element method for stress and deformation analyses of bi-directional functionally graded truncated conical shells, *Mechanics Based Design of Structures and Machines*, 48(4), 2020, 433-458.
[7] Abo-Bakr, H.M., Abo-Bakr, R.M., Mohamed, S.A., Eltaher, M.A., Weight optimization of axially functionally graded microbeams under buckling and vibration behaviors, *Mechanics Based Design of Structures and Machines*, 2020, 1-22. DOI: 10.1080/15397734.2020.1838298
[8] Abo-Bakr, H.M., Abo-bakr, R.M., Mohamed, S.A., Eltaher, M.A., Multi-objective shape optimization for axially functionally graded microbeams, *Composite Structures*, 258, 2021, 113370.
[9] Abo-Bakr, R.M., Abo-Bakr, H.M., Mohamed, S.A., Eltaher, M.A., Optimal weight for buckling of FG beam under variable axial load using Pareto optimality, *Composite Structures*, 258, 2021, 113193.
[10] Abo-bakr, R.M., Shanab, R.A., Attia, M.A., Multi-objective optimization for lightweight design of bi-directional functionally graded beams for maximum frequency and buckling load, *Composite Structures*, 278, 2021, 114691.
[11] Pham, Q.H., Nguyen, P.C., Tran, V.K., Nguyen-Thoi, T., Isogeometric analysis for free vibration of bidirectional functionally graded plates in the fluid medium, *Defence Technology*, 2021. DOI: 10.1016/j.dt.2021.09.006
[12] Attia, M.A., Shanab, R.A., Vibration characteristics of two-dimensional FGM nanobeams with couple stress and surface energy under general boundary conditions, *Aerospace Science and Technology*, 111, 2021, 106552.
[13] Shanab, R.A., Attia, M.A., On bending, buckling and free vibration analysis of 2D-FG tapered Timoshenko nanobeams based on modified couple stress and surface energy theories, *Waves in Random and Complex Media*, 2021, 1-47. DOI: 10.1080/17455030.2021.1884770
[14] Chen, X., Chen, L., Huang, S., Li, M., Li, X., Nonlinear forced vibration of in-plane bi-directional functionally graded materials rectangular plate with global and localized geometrical imperfections, *Applied Mathematical Modelling*, 93, 2021, 443-466.
[15] Hendi, A.A., Eltaher, M.A., Mohamed, S.A., Attia, M.A., Abdalla, A.W., Nonlinear thermal vibration of pre/post-buckled two-dimensional FGM tapered microbeams based on a higher order shear deformation theory, *Steel and Composite Structures*, 41(6), 2021, 787-802.
[16] Ohab-Yazdi, S.M.K., Kadkhodayan, M., Free vibration of bi-directional functionally graded imperfect nanobeams under rotational velocity, *Aerospace Science and Technology*, 119, 2021, 107210.
[17] Banh, T.T., Luu, N.G., Lieu, Q.X., Lee, J., Kang, J., Lee, D., Multiple bi-directional FGMs topology optimization approach with a preconditioned conjugate gradient multigrid, *Steel and Composite Structures*, 41(3), 2021, 385-402.
[18] Arasan, U., Venkatachalam, S., Murthy, H., Solution to two-dimensional elastic problems involving functionally graded material in radial co-ordinates, *Acta Mechanica*, 233, 2022, 343–362.
[19] Fu, P., Zhao, J., Zhang, X., Kang, G., Wang, P., Kan, Q., Elastic shakedown analysis of two-dimensional thermo-elastic rolling/sliding contact for a functionally graded coating/substrate structure with arbitrarily varying thermo-elastic properties, *Composite Structures*, 280, 2022, 114891.
[20] Brischetto, S., Torre, R., 3D Stress Analysis of Multilayered Functionally Graded Plates and Shells under Moisture Conditions, *Applied Sciences*, 12(1), 2022, 512.
[21] Barati, A., Hadi, A., Nejad, M.Z., Noroozi, R., On vibration of bi-directional functionally graded nanobeams under magnetic field, *Mechanics Based Design of Structures and Machines*, 50(2), 2022, 468-485.
[22] Whitney, J.M., Pagano, N.J., Shear deformation in heterogeneous anisotropic plates, *Journal of Applied Mechanics*, 37(4), 1970, 1031-1036.
[23] Reddy, J.N., Free vibration of antisymmetric, angle-ply laminated plates including transverse shear deformation by the finite element method, *Journal of Sound and Vibration*, 66(4), 1979, 565-576.
[24] Touratier, M., An efficient standard plate theory, *International Journal of Engineering Science*, 29(8), 1991, 901-916.
[25] Assie, A.E., Mahmoud, F.F., Dynamics of thick hygrothermal viscoelastic composite laminates through finite element method, *Structural Engineering and Mechanics*, 17(5), 2004, 727-734.
[26] Mantari, J.L., Oktem, A.S., Soares, C.G., Bending response of functionally graded plates by using a new higher order shear deformation theory, *Composite Structures*, 94(2), 2012, 714-723.
[27] Neves, A.M.A., Ferreira, A.J., Carrera, E., Cinefra, M., Jorge, R.M.N., Soares, C.M.M., Static analysis of functionally graded sandwich plates according to a hyperbolic theory considering Zig-Zag and warping effects, *Advances in Engineering Software*, 52, 2012, 30-43.
[28] Sedighi, H.M., Shirazi, K.H., Noghrehabadi, A.R., Yildirim, A., Asymptotic investigation of buckled beam nonlinear vibration, *Iranian Journal of Science and Technology, Transactions of Mechanical Engineering*, 36(M2), 2012, 107-116.
[29] Sedighi, H.M., Reza, A., Zare, J., The effect of quintic nonlinearity on the investigation of transversely vibrating buckled Euler-Bernoulli beams, *Journal of Theoretical and Applied Mechanics*, 51, 2013, 959-968.
[30] Mantari, J.L., Soares, C.G., A novel higher-order shear deformation theory with stretching effect for functionally graded plates, *Composites Part B: Engineering*, 45(1), 2013, 268-281.
[31] Assie, A.E., Kabeel, A.M., Mahmoud, F.F., Optimum design of laminated composite plates under dynamic excitation, *Applied Mathematical Modelling*, 36(2), 2012, 668-682.
[32] Yu, T., Yin, S., Bui, T.Q., Xia, S., Tanaka, S., Hirose, S., NURBS-based isogeometric analysis of buckling and free vibration problems for laminated composites plates with complicated cutouts using a new simple FSDT theory and level set method, *Thin-Walled Structures*, 101, 2016, 141-156.
[33] Nguyen, H.N., Hong, T.T., Vinh, P.V., Quang, N.D., Thom, D.V., A refined simple first-order shear deformation theory for static bending and free vibration analysis of advanced composite plates, *Materials*, 12(15), 2019, 2385.
[34] Vu, T.V., Nguyen, H.T., Nguyen-Van, H., Nguyen, T.P., Curiel-Sosa, J.L., A refined quasi-3D logarithmic shear deformation theory-based effective meshfree method for analysis of functionally graded plates resting on the elastic foundation, *Engineering Analysis with Boundary Elements*, 131, 2021, 174-193.
[35] Raissi, H., Stress analysis in adhesive layers of a five-layer circular sandwich plate subjected to temperature gradient based on layerwise theory, *Mechanics Based Design of Structures and Machines*, 2020, 1-27. DOI: 10.1080/15397734.2020.1776619
[36] Khiloun, M., Bousahla, A.A., Kaci, A., Bessaim, A., Tounsi, A., Mahmoud, S.R., Analytical modeling of bending and vibration of thick advanced composite plates using a four-variable quasi 3D HSDT, *Engineering with Computers*, 36(3), 2020, 807-821.
[37] Fallahi, N., Viglietti, A., Carrera, E., Pagani, A., Zappino, E., Effect of fiber orientation path on the buckling, free vibration, and static analyses of variable angle tow panels, *Facta Universitatis. Series: Mechanical Engineering*, 18(2), 2020, 165-188.
[38] Fallahi, N., GA optimization of variable angle tow composites in buckling and free vibration analysis through layerwise theory, *Aerospace*, 8(12), 2021, 376.
[39] Arshid, E., Khorasani, M., Soleimani-Javid, Z., Amir, S., Tounsi, A., Porosity-dependent vibration analysis of FG microplates embedded by polymeric nanocomposite patches considering hygrothermal effect via an innovative plate theory, *Engineering with Computers*, 2021, 1-22. DOI: 10.1007/s00366-021-01382-y
[40] Pham, Q.H., Tran, V.K., Tran, T.T., Nguyen-Thoi, T., Nguyen, P.C., A nonlocal quasi-3D theory for thermal free vibration analysis of functionally graded material nanoplates resting on elastic foundation, *Case Studies in Thermal Engineering*, 26, 2021, 101170.
[41] Pavlovic, A., Fragassa, C., Minak, G., Buckling analysis of telescopic boom: theoretical and numerical verification of sliding pads, *Tehnički Vjesnik*, 24(3), 2017, 729-735.
[42] Daikh, A.A., Houari, M.S.A., Eltaher, M.A., A novel nonlocal strain gradient Quasi-3D bending analysis of sigmoid functionally graded sandwich nanoplates, *Composite Structures*, 262, 2021, 113347.
[43] Daikh, A.A., Houari, M.S.A., Belarbi, M.O., Chakraverty, S., Eltaher, M.A., Analysis of axially temperature-dependent functionally graded carbon nanotube reinforced composite plates, *Engineering with Computers*, 2021, 1-22. DOI: 10.1007/s00366-021-01413-8
[44] Li, M., Soares, C.G., Yan, R., Free vibration analysis of FGM plates on Winkler/Pasternak/Kerr foundation by using a simple quasi-3D HSDT, *Composite Structures*, 264, 2021, 113643.
[45] Van Vinh, P., Deflections, stresses and free vibration analysis of bi-functionally graded sandwich plates resting on Pasternak's elastic foundations via a hybrid quasi-3D theory, *Mechanics Based Design of Structures and Machines*, 2021, 1-32. DOI: 10.1080/15397734.2021.1894948
[46] Sadgui, A., Tati, A., A novel trigonometric shear deformation theory for the buckling and free vibration analysis of functionally graded plates,

Mechanics of Advanced Materials and Structures, 2021, 1-16. DOI: 10.1080/15376494.2021.1983679
[47] Li, M., Yan, R., Xu, L., Soares, C.G., A general framework of higher-order shear deformation theories with a novel unified plate model for composite laminated and FGM plates, *Composite Structures*, 261, 2021, 113560.
[48] Tran, T.T., Nguyen, P.C., Pham, Q.H., Vibration analysis of FGM plates in thermal environment resting on elastic foundation using ES-MITC3 element and prediction of ANN, *Case Studies in Thermal Engineering*, 24, 2021, 100852.
[49] Sofiyev, A.H., Dikmen, F., Buckling Analysis of Functionally Graded Shells under Mixed Boundary Conditions Subjected to Uniform Lateral Pressure, *Journal of Applied and Computational Mechanics*, 7(1), 2021, 345-354.
[50] Civalek, Ö., Avcar, M., Free vibration and buckling analyses of CNT reinforced laminated non-rectangular plates by discrete singular convolution method, *Engineering with Computers*, 38, 2022, 489–521.
[51] Hamed, M.A., Abo-Bakr, R.M., Mohamed, S.A., Eltaher, M.A., Influence of axial load function and optimization on static stability of sandwich functionally graded beams with porous core, *Engineering with Computers*, 36(4), 2020, 1929-1946.
[52] Abdollahi, M., Saidi, A.R., Bahaadini, R., Aeroelastic analysis of symmetric and non-symmetric trapezoidal honeycomb sandwich plates with FG porous face sheets, *Aerospace Science and Technology*, 119, 2021, 107211.
[53] Sobhy, M., Zenkour, A.M., Porosity and inhomogeneity effects on the buckling and vibration of double-FGM nanoplates via a quasi-3D refined theory, *Composite Structures*, 220, 2019, 289-303.
[54] Coskun, S., Kim, J., Toutanji, H., Bending, free vibration, and buckling analysis of functionally graded porous micro-plates using a general third-order plate theory, *Journal of Composites Science*, 3(1), 2019, 15.
[55] Kim, J., Zur, K.K., Reddy, J.N., Bending, free vibration, and buckling of modified couples stress-based functionally graded porous micro-plates, *Composite Structures*, 209, 2019, 879-888.
[56] Babaei, M., Asemi, K., Kiarasi, F., Static response and free-vibration analysis of a functionally graded annular elliptical sector plate made of saturated porous material based on 3D finite element method, *Mechanics Based Design of Structures and Machines*, 2020, 1-25. DOI: 10.1080/15397734.2020.1864401
[57] Esmaeilzadeh, M., Golmakani, M.E., Sadeghian, M., A nonlocal strain gradient model for nonlinear dynamic behavior of bi-directional functionally graded porous nanoplates on elastic foundations, *Mechanics Based Design of Structures and Machines*, 2020, 1-20. DOI: 10.1080/15397734.2020.1845965
[58] Cho, I.H., Wave energy dissipation by a floating horizontal porous plate in oblique incident waves, *Wave Motion*, 105, 2021, 102765.
[59] Hieu, D.V., Chan, D.Q., Sedighi, H.M., Nonlinear bending, buckling and vibration of functionally graded nonlocal strain gradient nanobeams resting on an elastic foundation, *Journal of Mechanics of Materials and Structures*, 16(3), 2021, 327-346.
[60] Katiyar, V., Gupta, A., Vibration response of a geometrically discontinuous bi-directional functionally graded plate resting on elastic foundations in thermal environment with initial imperfections, *Mechanics Based Design of Structures and Machines*, 2021, 1-29. DOI: 10.1080/15397734.2021.1929313
[61] Akbas, S.D., Bashiri, A.H., Assie, A.E., Eltaher, M.A., Dynamic analysis of thick beams with functionally graded porous layers and viscoelastic support, *Journal of Vibration and Control*, 27(13-14), 2021, 1644-1655.
[62] Akbas, S.D., Fageehi, Y.A., Assie, A.E., Eltaher, M.A., Dynamic analysis of viscoelastic functionally graded porous thick beams under pulse load, *Engineering with Computers*, 38, 2022, 365–377.
[63] Sah, S.K., Ghosh, A., Influence of porosity distribution on free vibration and buckling analysis of multi-directional functionally graded sandwich plates, *Composite Structures*, 279, 2022, 114795.
[64] Karama, M., Afaq, K.S., Mistou, S., Mechanical behaviour of laminated composite beam by the new multi-layered laminated composite structures model with transverse shear stress continuity, *International Journal of Solids and Structures*, 40(6), 2003, 1525-1546.
[65] Thai, H.T., Kim, S.E., Closed-form solution for buckling analysis of thick functionally graded plates on elastic foundation, *International Journal of Mechanical Sciences*, 75, 2013, 34-44.
[66] Taibi, F.Z., Benyoucef, S., Tounsi, A., Bachir Bouiadjra, R., Adda Bedia, E.A., Mahmoud, S.R., A simple shear deformation theory for thermo-mechanical behaviour of functionally graded sandwich plates on elastic foundations, *Journal of Sandwich Structures & Materials*, 17(2), 2015, 99-129.
[67] Bellman, R., Kashef, B.G., Casti, J., Differential quadrature: a technique for the rapid solution of nonlinear partial differential equations, *Journal of Computational Physics*, 10(1), 1972, 40-52.
[68] Shu, C., *Differential quadrature and its application in engineering*, Springer Science & Business Media, 2012.
[69] Zong, Z., *Advanced differential quadrature methods*, Chapman and Hall/CRC, 2009.
[70] Mohamed, S.A., A fractional differential quadrature method for fractional differential equations and fractional eigenvalue problems, *Mathematical Methods in the Applied Sciences*, 2020, DOI: 10.1002/mma.6753
[71] Mohamed, S.A., Mohamed, N.A., Abo-Hashem, S.I., A novel differential-integral quadrature method for the solution of nonlinear integro-differential equations, *Mathematical Methods in the Applied Sciences*, 44(18), 2021, 13945-13967.
[72] Thai, H.T., Choi, D.H., An efficient and simple refined theory for buckling analysis of functionally graded plates, *Applied Mathematical Modelling*, 36(3), 2012, 1008-1022.

ORCID iD

Amr E. Assie https://orcid.org/0000-0002-7811-5591
Salwa A. Mohamed https://orcid.org/0000-0001-8894-1347
Rabab A. Shanab https://orcid.org/0000-0001-6965-3729
Rasha M. Abo-bakr https://orcid.org/0000-0002-5868-3778
Mohamed A. Eltaher http://orcid.org/0000-0003-3116-2101

How to cite this article: Assie A.E., Mohamed S.A., Shanab R.A., Abo-bakr R.M., Eltaher M.A. Static Buckling of 2D FG Porous Plates Resting on Elastic Foundation based on Unified Shear Theories , *J. Appl. Comput. Mech.*, 9(1), 2023, 239–258. https://doi.org/10.22055/jacm.2022.41265.3723